國 立 交 通 大 學
光 電 工 程 研 究 所

碩 士 論 文

硒化鎵晶體中兆赫波光參數放大之研究

The study of terahertz optical parametric

amplification in ε -GaSe crystals

研 究 生：許哲睿

指 導 老 師：潘犀靈 教授

中 華 民 國 九 十 六 年 七 月

硒化鎵晶體中兆赫波光參數放大之研究

The study of terahertz optical parametric

amplification in ε -GaSe crystals

研 究 生：許哲睿　　　　　　　Student：Che-Jui Hsu

指導老師：潘犀靈 教授　　　　　Advisor：Prof. Ci-Ling Pan

國立交通大學
光電工程研究所
碩士論文

A Dissertation
Submitted to Department of Photonics and
Institute of Electro-Optical Engineering
College of Electrical Engineering and Computer Science
National Chiao Tung University
In partial Fulfillment of the Requirements
For the Degree of
Master of Engineering
In

Electro-Optical Engineering
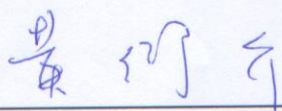
July 2007
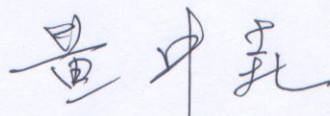Hsinchu, Taiwan, Republic of China

中 華 民 國 九 十 四 年 七 月

國 立 交 通 大 學

論 文 口 試 委 員 會 審 定 書

本校　光電工程研究所　碩士班　　　許哲睿　　君
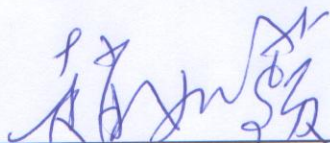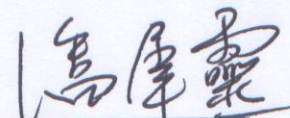
所提論文：　硒化鎵晶體中兆赫波光參數放大之研究

合於碩士資格水準、業經本委員會評審認可。

口試委員：

黃衍介 教授　　　　　　黃中垚 教授

趙如蘋 教授

指導教授：

潘犀靈 教授

所　長：　　　　　　　　　教授

系主任：　　　　　　　　　教授

中 華 民 國 九十六 年 七 月 十六 日

硒化鎵晶體中兆赫波光參數放大之研究

研究生：許哲睿　　　　　　　　　　　　　指導教授：潘犀靈　教授

國立交通大學光電工程研究所

摘　要

　　以兆赫波時域光譜技術測量純的及摻鉺的硒化鎵晶體在兆赫波段的光學性質，我們發現二者的折射率在 0.2-1.2THz 波段約為 3.2，純硒化鎵晶體的吸收係數平均為 $5\,cm^{-1}$，摻鉺的硒化鎵晶體的吸收係數平均為 $55\,cm^{-1}$，二者在 0.589 THz 處都有一聲子吸收峯。利用 Lorentz-Drude model 計算其導電率並以理論擬合可得知此二晶體的弛緩率及平均碰撞時間，我們進一步推算其載子遷移率分別為 $\mu = 81 cm^2/Vs$ 及 $\mu = 39\,cm^2/Vs$。

　　我們也架設了一套由高功率飛秒雷射聚焦游離空氣產生電漿，以空氣的三階非線性係數滿足四波混頻的兆赫波產生源。改變雷射基頻(800 nm)及二倍頻(400 nm)間的相位差、偏振方向夾角及強度，量測其產生的兆赫波的特性。並利用此光源來作硒化鎵晶體中兆赫波光參數放大的研究，初步結果顯示在 1THz 此光參數放大器有 150% 的增益。

The study of terahertz optical parametric amplification in ε-GaSe crystals

Student: Che-Jui Hsu   Advisor: Prof. Ci-Ling Pan

Institute of Electro-Optical Engineering
College of Electrical Engineering and Computer Science
National Chiao Tung University

Abstract

Optical constants of pure and 0.2% Er:GaSe in 0.2 – 1.2 THz region are determined by THz-TDS. The refractive indexes for both crystals are 3.2 and absorption coefficients are $5\,cm^{-1}$ and $55\,cm^{-1}$, respectively. A phonon vibration is observed at 0.589 THz for both crystals. By use of Lorentz – Drude model, the conductivity can be further calculated from experimental measurement. The parameters such as relaxation rate and momentum relaxation time are also derived. The mobility $\mu = 81\,cm^2/Vs$ for pure GaSe and $\mu = 39\,cm^2/Vs$ for Er:GaSe are also proposed.

Femtosecond Laser induced plasma based on the third order nonlinearity is successfully utilized to construct the THz-TDS. The properties of the THz radiation from this configuration is characterized by altering the phase difference, the angle of polarization and intensity between fundamental beam (800nm) and second harmonic beam (400nm). Terahertz enhancement/amplification is preliminarily performed in our studies. The gain could be as high as 150% under the phase matching condition around 1THz.

Acknowledgement

首先誠摯的感謝指導教授潘犀靈老師，老師提供良好的實驗環境及細心的指導，使我在求學的過程中學到不少專業知識及研究方法。

在實驗上耐心教導我的陳晉瑋學長，學長淵博的學識以及實驗嚴謹的精神，對我的研究態度有了很大的影響；感謝王怡超學長在雷射系統的維護及調整，讓我有穩定的雷射光源進行實驗；謝卓帆學長及黎宇泰學長在系統使用上的教導及建議。

此外感謝這二年來一起奮鬥的同學昀浦、韋文、彥毓、宜貞、君豪，不僅在課業及實驗上的幫助，也給予我不少生活的美好回憶。學弟妹，育賢、介暐、孟桓、松輝、綿綿、峻維的加入，也為生活增添了不少歡樂。

最後我要感謝我的家人，總是在背後默默的支持，沒有你們的栽培就沒有今日的我。

Table of Contents

List of Figures

List of Tables

Chapter 1

Overview of Terahertz Radiation

1.1 Introduction

After the rapid progress in ultrafast lasers and the successes in semiconductor technology and nonlinear optics, it has leaded the birth of a new area of applied physics known as optoelectronics or photonics in 1970s. One of the most promising photonic spectroscopic applications, is the terahertz time-domain spectroscopy (THz-TDS), is now barely 15 years old.
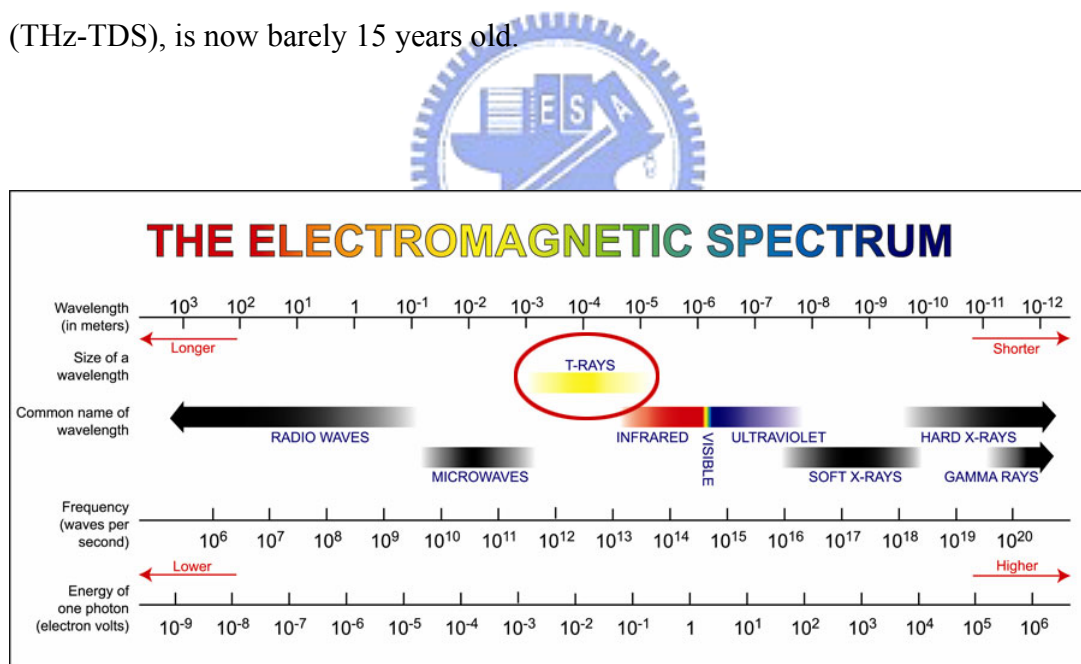
Figure 1-1 : Overview of frequency regions. [1]

1 THz can be presented as: 1 THz = 1 ps = $300\ \mu m$ = 33 cm^{-1} = 4.1 meV = 47.6K. Even though the terahertz (THz) region lies between microwave and infrared regions is relatively narrow (see Figure 1-1), it is important in condensed matter physics.

There are as many interesting phenomena falling right to this region, especially the soft lattice vibrations in dielectrics. The microwave wave region can be accessible via conventional radiofrequency methods, which cannot be extended as the frequency of synthesizers is limited. In the infrared region, the optical devices are used, however, while the frequency is lowered, the brightness of common infrared radiation sources practically vanishes.

The development and spread of THz sources and receiver advance the THz time-domain spectroscopy. Table 1-1 is the list of common use of THz emitter and detector. As the THz spectroscopy is a time-domain method, the pump-probe experiments can be easily performed. The sample can be excited by the optical pump beam, which is split from the femtosecond laser beam the pump beam is perfectly synchronized with the THz probe pulse and gating pulse. During last few years, the femtosecond optical amplifiers and parametric generators became commercially available. The regenerative amplified laser enabled us to generate a very intense excitation pulse and the latter to tune the excitation wavelength. This makes the THz time-domain spectroscopy very suitable for investigations of ultrafast dynamics on the subpicosecond time scale.

Table 1-1 : List of THz emitters and detectors and their advantage

Emitter	Type	Advantage
	Free electron laser	Highest THz power
	Gunn oscillator	Generate sub THz
	Quantum cascade laser	CW, single mode

	Differential frequency generation	Narrow linewidth CW possible
	Photoconductive antenna	High SNR
	Semiconductor surfaces	Higher THz power
	Optical rectification	broadband THz spectrum
Detector	**Type**	**Advantage**
	Bolometer	incoherent radiation, more sensitivity
	Pyroelectric detector	incoherent radiation
	Photoconductive dipole antenna	Higher SNR
	Electro-optic crystal	broadband THz spectrum

In recent years, THz spectroscopy systems have been applied to a variety of domains, such as material characterization, image and tomography, biomaterial application. The ability of THz-TDS to measure both real and imaginary components of the dielectric function in real time has made it a desired method to study the materials at THz frequencies. THz spectroscopy in chemistry and biology is another area of studies. Rotational, bending, and torsion dynamics of molecules can be probed by THz waves. In addition to the gas phase, the dynamics of molecules in condensed phases can be studied. Using subpicosecond waves one can study relaxation processes, and high THz fields can induce interionic motion or molecular orientational motion, changing the local structure. Imaging is also a very promising field of study and application. THz radiation can be applied to medical imaging of skin, teeth, etc. Unique biological

resonances are the basis for THz signature imaging employed to identify disease. Pharmacists can also benefit from THz spectroscopy. Drugs can be differentiated and identified using THz spectroscopy by different forms of the same compound with different pharmaceutical activities.

1.2 Terahertz Generation Methods

1.2.1 Generation by Optical rectification

The generation of terahertz by optical rectification method is only possible by pulsed laser. Optical rectification is the generation of DC polarization by the application of optical waves in a non-centrosymmetric medium with large second order susceptibility $\chi^{(2)}$.

Assume a femtosecond pumping pulse propagates in z-direction, pulse duration τ_G with Gaussian profile.

$$I(\omega) = I_0(\omega)\exp(-(\tau_G\omega)^2/2) \tag{1}$$

When it propagates through the nonlinear optical crystal, there will be induced polarization in the crystal

$$P^{(2)}(z,\omega) = \chi^{(2)}(\omega)I(\omega)\exp(-\omega z/v_g) \tag{2}$$

where v_g is the group velocity of pump pulse.

By solving nonlinear Maxwell's equations

$$-\nabla^2 E + \frac{1}{c^2}\frac{\partial^2 D^{(1)}}{\partial t^2} = -\frac{4\pi}{c^2}\frac{\partial^2 P^{(2)}}{\partial t^2} \tag{3}$$

The locally generated terahertz electric field

$$E_{THz}(z,\omega) = \omega^2 \chi^{(2)}(\omega) z \, sinc(\Delta k_{THz} z/2) \tag{4}$$

Then the generated terahertz is integral of local generation.

If these are no momentum mismatch, the output signal follows the intensity envelope of the pump laser pulse. For example, we use 100 fs pulses as the pump. The spectrum of the generated pulse peaks around a few terahertz.

Because the ultrafast pulses have large bandwidth, the frequency components are differentiated with each other and the produced signal have frequency component from 0 to the bandwidth of the pump $\Delta\omega \sim \dfrac{1}{\tau_G} \sim 10\,THz$. The current record for THz detection is 70THz [2]. Figure 1-2 illustrates the terahertz radiation generated by optical rectification.
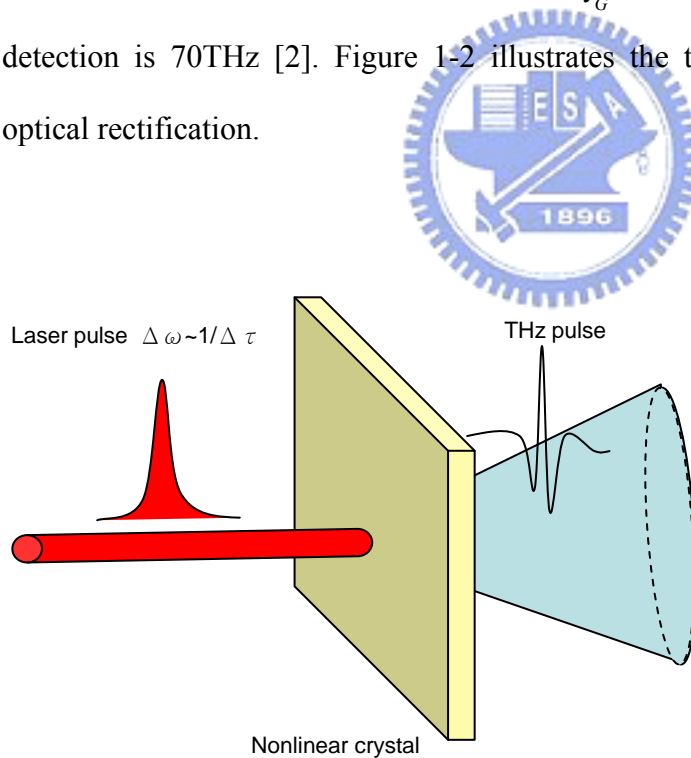
Figure 1-2 : Illustration of terahertz radiation by optical rectification

1.2.2   Generation by Photoconductive Antenna

Femtosecond laser excites a biased semiconductor with photon energies greater than its bandgap, will produce electrons and holes at the illumination point in the conduction and valence bands (Figure 1-3). Owing to fast changing of the density of the carriers and accelerated by the applied dc bias, electromagnetic field radiating into free-space. The production of currents with a full-width half-maximum (FWHM) of 1ps (or less) depends on the carrier lifetime in the semiconductor [3].
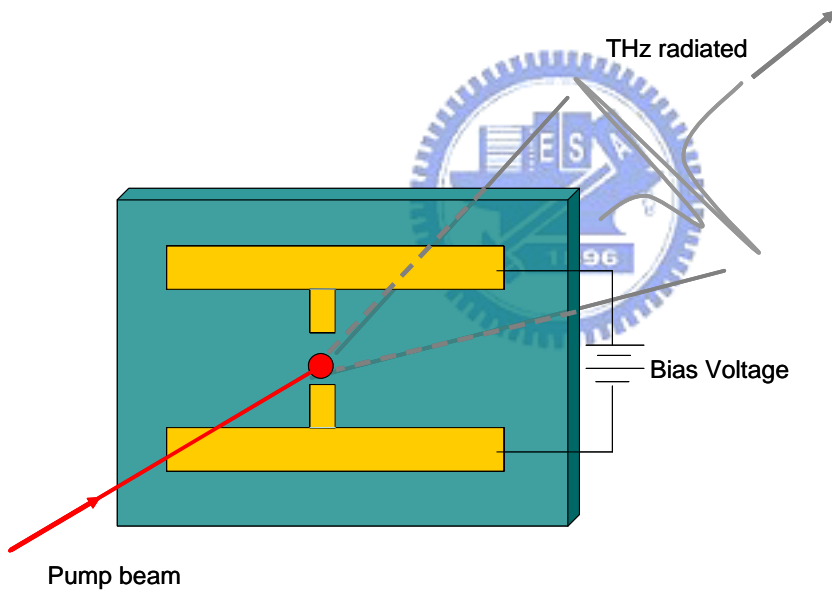
Figure 1-3 : Schematic of PC antenna

The carrier density behavior in time is given by

$$dn/dt = -n/\tau_t + G(t)$$

(5)

where n is the carrier density and $G(t) = n_0 \exp(t/\Delta t)^2$ is the generation rate of

carriers due to laser pulse excitation, with Δt the laser pulse width and n_0 the generated carrier density at $t = 0$. The generated carriers are accelerated by the bias field with a velocity rate given by

$$dv_{e,h}/dt = -v_{e,h}/\tau_{rel} + (q_{e,h}E)/m_{eff,e,h} \tag{6}$$

where $v_{e,h}$ are the average velocity of the carrier, $q_{e,h}$ are the charge of the electron and hole, τ_{rel} is the momentum relaxation time, and E is the local electric field, which is less than the applied bias E_b because of the screen effect of space charges. The relation is

$$E = E_b - P/3\varepsilon_r \tag{7}$$

where ε_r is the dielectric constant and P is the polarization induced by the separation of electrons and holes. The polarization depends on time according to the expression

$$dP/dt = -P/\tau_{rec} + J \tag{8}$$

where τ_{rec} is the recombination time between electrons and holes ($\tau_{rec} = 10$ ps for LT-GaAs) and $J = env_h + (-e)nv_e$ is the current density.

The far-field radiation is given by

$$E_{THz} \propto \partial J/\partial t \propto ev\partial n/\partial t + en\partial v/\partial t, \tag{9}$$

where $v = v_e - v_h$. The transient electromagnetic field E_{THz} consists of two terms: the first term describes the carrier density charge effect while the second term describes the effect of charge acceleration due to the electric field bias.

1.2.3 Generation by laser induced plasma

In 1993, Hamster et al. first observed terahertz emission from laser-induced plasmas. This is a very novel method of generating terahertz which is emitting from laser induced plasma based on amplified laser systems. The basic concept of these emitters is to focus an ultrafast high energy laser pulse in a gaseous medium such as ambient air. Reaching optical field strengths as high as $5 \times 10^{14} \, W/cm^2$ which is enough to ionize the air and form a plasma in the focal region.

Up to now, there are three different methods to generating terahertz from plasma as our knowledge:

1. Emission based on ponderomotive force

The mechanism is that the polarization produced by the free electrons that are accelerated by the ponderomotive forces associated with the propagating laser pulse, i.e. due to a spatio-temporal optical intensity gradient within the plasma. In this method, a rotationally symmetric polarization is created around the beam propagation axis, this leads to an emission of terahertz radiation in a diverging cone about the optical propagation axis. Due to symmetry reasons no net terahertz field radiates along the optical propagation axis. [4]

Compared to other two methods employing laser-induced, the pulse energy of the terahertz generated by this method is relatively low.

2. Emission based on external bias fields

This method is applying an external bias field to the plasma region. It can increase the terahertz radiation strength and to direct it into the forward direction of the optical propagation axis. The terahertz pulse amplitude scales linearly with the external bias

field. The maximum achievable terahertz pulse energy for a given laser pulse energy is limited by the maximum external bias field. [5]

3. Emission based on optical second harmonic bias

This method is more efficient than above two, when laser pulses composed of a superposition of both fundamental and second harmonic spectral components which are focused into air.

Cook et al. initially attributed the terahertz generation process to four-wave rectification mediated by the third order nonlinearity of air [6] but later reported indications for a plasma-driven process [7]. In the four wave rectification process, the frequencies of the three input beams add to nearly zero (THz frequency) and the nonlinear polarization in the focal region and respectively the terahertz field amplitude are given by

$$E_{THz}(t) \propto P_{plasma} \propto \chi^{(3)} E_{2\omega} E_{\omega}^*(t) E_{\omega}^*(t) \cos(\varphi) \tag{10}$$

Where $\chi^{(3)}(\Omega : 2\omega + \Omega, -\omega, -\omega)$ is the third order susceptibility, E_{ω} and $E_{2\omega}$ is the electric field of fundamental wave and the second harmonic wave, respectively. $\varphi = k_{2\omega} \Delta l$ is the phase difference between the fundamental and second harmonic beams, $k_{2\omega}$ is the wave vector of the second harmonic beam and Δl is the path difference between the fundamental wave and the second harmonic wave along the beam propagation direction.

1.3 Terahertz Detection Methods

1.3.1 Detection by Photoconductive Antenna

In 1984, Auston first generated and detected the THz pulses by photoconductive antennas [8]. In photoconductive antennas detection the antenna is gated with a femtosecond pulse. The gating pulse creates carriers and the terahertz pulse provides the bias field to create a detectable current in the detection antenna. The output polarity is sensitive to the direction of the field. The output is typically connected to a computer via a lock-in amplifier so that when the delay of the gate pulse is scanned over a several picoseconds region the electric field of the terahertz pulse is mapped out on the screen. For several years it was thought that the length of the optical gating pulse and the decay rate of the semiconductor were crucial to the detector responsivity and time resolution. It was therefore assumed that no advantage could be gained from using shorter gating pulses, as the carrier lifetime of the carriers would always determine the response time of the detector. This in turn would therefore limit the detection capability of a typical GaAs photoconductive antenna to low frequencies.
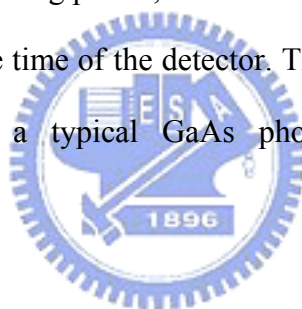
1.3.2   Detection by Electric Optical Sampling

In 1995, the free space electric optical sampling (FEOS) detection scheme was first introduced by the groups of X.-C. Zhang. [9] This method has widely used and allowed for coherent detection of the temporal evolution of the electric field in the ultrashort transients.
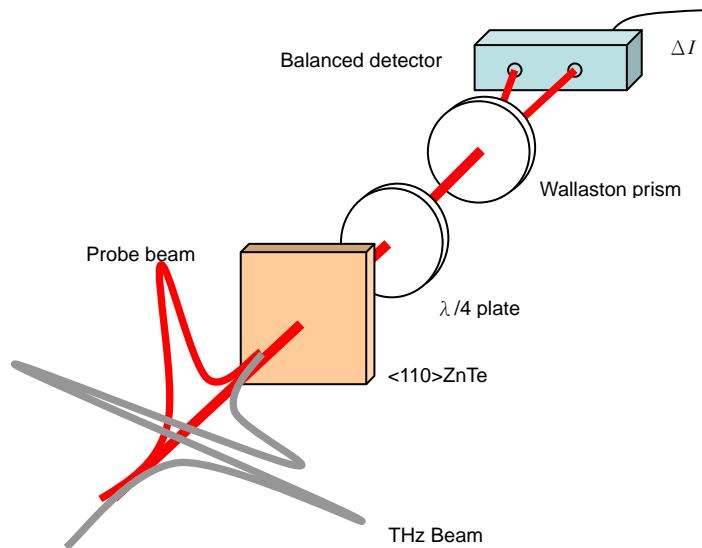
Figure 1-4 : The scheme of EO sampling setup

Figure 1-4 is the schematic of FEOS setup, it consists of EO crystal, quarter wave plate (or compensator), wallaston prism, balanced detector.

First, when there is no terahertz field present, the optical probe beam will not be affected by the EO crystal, then by rotating the angle of quarter wave plate, to make the polarization become circularly. This circularly polarized beam will be split into two orthogonal polarization components (*s*- and *p*-polarization) with equal intensity. The balanced detector measures the intensity difference between these two components, the value is zero. When terahertz meet the EO crystal, the electric field of a teraherz pulse will induce a small birefringence in an EO crystal through Pockels effect. Passing through such crystal, the initially linearly polarized optical probe beam will change into elliptical polarization. This ellipticity is proportional to the electric field which applied to the crystal. Then the elliptical polarization probe beam will be split into two orthogonal polarization parts by wallaston prism. The difference can be detected by balanced detector, terahertz amplitude is proportional to the signal. In

general, the duration of terahertz pulse is several picosecond (or subpicosecond) much longer than the laser pulse (femtosecond order), the terahertz field can be approximately treated as a dc bias field. Thus, by scanning the delay between terahertz and probe beam the whole terahertz time domain profile can be figured out.

The balanced detection signal for an EOS crystal such as <110> ZnTe can be calculated. ZnTe is a very common EO crystal used in terahertz EO sampling. It belongs to zinc-blende structure with $\overline{4}3m$ point group symmetry, the only nonzero coefficient of the electro tensor is γ_{41}.

$$\gamma_{ij} = \begin{bmatrix} 0 & 0 & 0 \\ 0 & 0 & 0 \\ 0 & 0 & 0 \\ \gamma_{41} & 0 & 0 \\ 0 & \gamma_{41} & 0 \\ 0 & 0 & \gamma_{41} \end{bmatrix} \tag{11}$$

$$\gamma_{41} = 3.9 \ pm/V$$

Here describe the angle ψ dependence of the signal in EO sampling with (110) ZnTe. When an arbitrary electric field $\vec{E} = (E_x, E_y, E_z)$ propagate along the (110) axis is applied to the EO crystal, in the crystal axes coordinate system (x, y, z), the refractive index ellispsoid can be written as

$$\frac{x^2 + y^2 + z^2}{n_o^2} + 2\gamma_{41}E_x yz + 2\gamma_{41}E_y zx + 2\gamma_{41}E_z xy = 1 \tag{12}$$

After rotating the (x, y, z) coordinate system around the z axis by 45°, the equation (12) becomes:
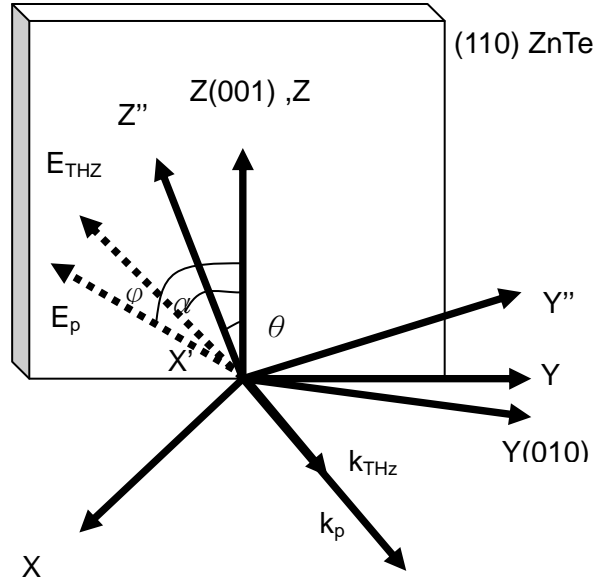
Figure 1-5 : Angles of the THz wave and probe beam polarization directions

$$\frac{1}{n_o^2}(\frac{1}{2}\sqrt{2}x' - \frac{1}{2}\sqrt{2}y')^2 + \frac{1}{n_o^2}(\frac{1}{2}\sqrt{2}x' + \frac{1}{2}\sqrt{2}y')^2 + \frac{z'}{n_o^2} + 2E_x r_{41}(\frac{1}{2}\sqrt{2}x' + \frac{1}{2}\sqrt{2}y')z'$$
$$+2E_y r_{41}(\frac{1}{2}\sqrt{2}x' - \frac{1}{2}\sqrt{2}y')z' + 2E_z r_{41}(\frac{1}{2}x'^2 - \frac{1}{2}y'^2) = 1$$

(13)

And $E_y = -E_x$

$$x'^2(\frac{1}{n_o^2} + E_z r_{41}) + y'^2(\frac{1}{n_o^2} - E_z r_{41}) + \frac{z'^2}{n_o^2} + 2\sqrt{2}E_x r_{41}y'z' = 1$$

(14)

Then the $(x^{'}, y^{'}, z^{'})$ coordinate system is rotated around the x' axis by θ :

$$x' = x''$$
$$y' = y''\cos\theta - z''\sin\theta$$
$$z' = y''\sin\theta + z''\cos\theta$$

(15)

The components of the electric field are expressed in terms of the angle α (the angle

of the THz beam polarization with respect to the (001) axis) shown in Figure 1-5.

$$E_z = E_{THz} \cos \alpha$$

$$E_x = E_{THz} \frac{\sqrt{2}}{2} \sin \alpha \tag{16}$$

With these definitions and some calculations, the index ellipsoid of Eq. (14) becomes:

$$x''^2 (\frac{1}{n_o^2} + E_{THz} r_{41} \cos \alpha) + y''^2 \{\frac{1}{n_o^2} - E_{THz} r_{41} [\cos \alpha \sin^2 \theta + \cos(\alpha + 2\theta)]\}$$

$$+ z''^2 \{\frac{1}{n_o^2} - E_{THz} r_{41} [\cos \alpha \cos^2 \theta - \cos(\alpha + 2\theta)]\} = 1 \tag{17}$$

And

$$2\theta = -\tan^{-1}(2 \tan \alpha) - n\pi$$

$$(n - \frac{1}{2})\pi \le \alpha < (n + \frac{1}{2})\pi, n = 0,1... \tag{18}$$

By setting $x'' = 0$ ($y'' z''$ $plane$), then solve the equation, we can get two eigenvalues.

$$\lambda_{1,2} = \frac{1}{n_0^2} - \gamma_{41} E_{THz} [\cos \alpha \sin^2 \theta \pm \cos(\alpha + 2\theta)] \tag{19}$$

The refractive indices for visible-near IR light propagating along the x''
direction are:

$$n_{y''}(\alpha) \approx n_0 + \frac{n_0^3}{2} E_{THz} r_{41} [\cos \alpha \sin^2 \theta + \cos(\alpha + 2\theta)]$$

$$n_{z''}(\alpha) \approx n + \frac{n_0^3}{2} E_{THz} r_{41} [\cos \alpha \cos^2 \theta - \cos(\alpha + 2\theta)] \tag{20}$$

The intensity detected by balance detector can be expressed as:

$$\Delta I(\alpha, \varphi) = I_p \sin[2(\varphi - \theta)] \sin\{\frac{\omega}{c} [n_{y''}(\alpha) - n_{z''}(\alpha)]L\}$$

$$= I_p \frac{\omega n_o^3 E_{THz} r_{41} L}{2c} (\cos \alpha \sin 2\varphi + 2 \sin \alpha \cos 2\varphi) \tag{21}$$

where L is crystal length, φ is the angle of the probe beam polarization with respect to the (001) axis shown in Figure 1-5.

The optimum signal can be realized at the largest phase retardation if $\alpha + 2\theta = n\pi, n = 0, \pm 1, \pm 2...$ which means terahertz beam should be parallel or perpendicular to probe beam to get maximum detected signal.

1.4 Laser System Used

Figure 1-6 is the laser setup which is consisted of a Spectra-Physics Millennia V diode-pumped laser that generates 5W of green light that pumps a Tsunami Titanium-doped sapphire laser with output of approximately 35 fs pulses at 800nm. The pulse repetition rate is 82 MHz and the output power is up to 500 mW.

800 nm, 50 fs, 2mJ

Empower

Ti:Sapphire Regenerative amplifier
(Spitfire, Spectra-Physics)

Millennia V

Ti:Sapphire laser
(Tsunami, Spectra-Physics)

800 nm, 35fs, 500mW
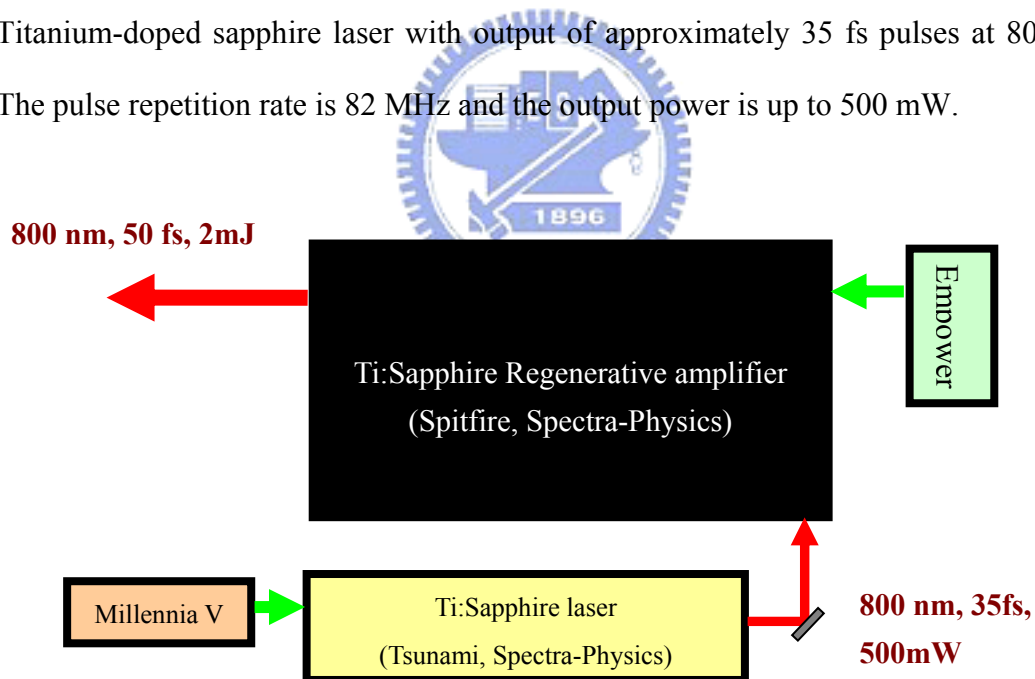
Figure 1-6 : The scheme of femtosecond laser system

The Ti:Sapphire beam is then directed into the Spitfire Ti:Sapphire regenerative amplifier system as the seeder. The pump beam for the amplification process in the Spitfire is Spectra-Physics Empower, a frequency doubled diode-pumped Nd:YLF

laser (527nm). The Spitfire amplifies the original seed pulses by a million times from 3nJ of energy per pulse to 2mJ per pulse, repetition rate 1KHz, or generates 20mJ pulse energy at repetition rate of 10Hz. Table 1-2 is the description of Tsunami and Spitfire.

Table 1-2 : The description of Tsunami and Spitfire

Laser	Tsunami	Spitfire	
Repetition rate	82MHz	1KHz	10Hz
Wavelength	800nm	800nm	800nm
Pulse duration	35fs	50fs	50fs
Pulse energy	6nJ	2mJ	20mJ

1.5 The Characteristics of THz Generated by Laser Induced Plasma by Four Wave Mixing

With the coming of the amplified laser system, one can easily reach pulse energy sufficient to ionize atoms and molecule in ambient air in the focused beam. If it is in an ambient air at 1 atm pressure, a plasma can be generated with a length of a few millimeter and a diameter of up to 100 μm can be produced by a 1 kHz Ti:Sapphire amplified laser system with pulse energies in the few hundreds of micro-joule regime.
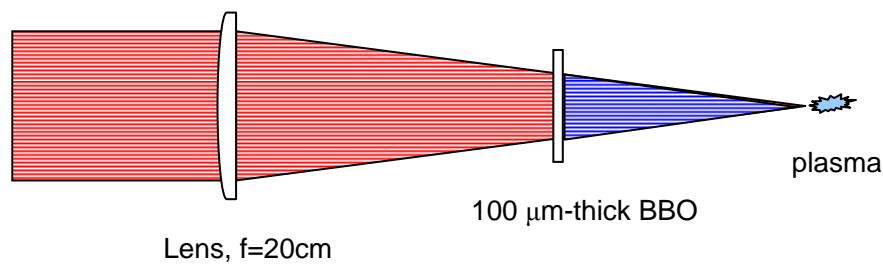
Figure 1-7 : Schematic of the laser induced plasma setup used for THz generation

Following the approach of Cook et al.[10], we construct a setup of terahertz time domain spectroscopy system with laser induced plasma to generate terahertz. Figure 1-7 is the illustration of terahertz generation setup, we employed 1kHz Ti:sapphire laser system (Spitfire) at 800nm with maximum pulse energy of $2\,m$J, pulse duration 50fs. We focus the pluses through a $100\,\mu m$ thick type-I β-barium borate (BBO) crystal with a lens (f=20$\,cm$), which has been phase matched for second harmonic generation (SHG), placed at an adjustable distance from the focus point. The generated terahertz is detected by free space EO sampling with $1\,mm$ thick ZnTe crystal. The terahertz time domain electric field is shown in Figure 1-8, and its corresponding frequency domain spectrum is depicted in the inset.
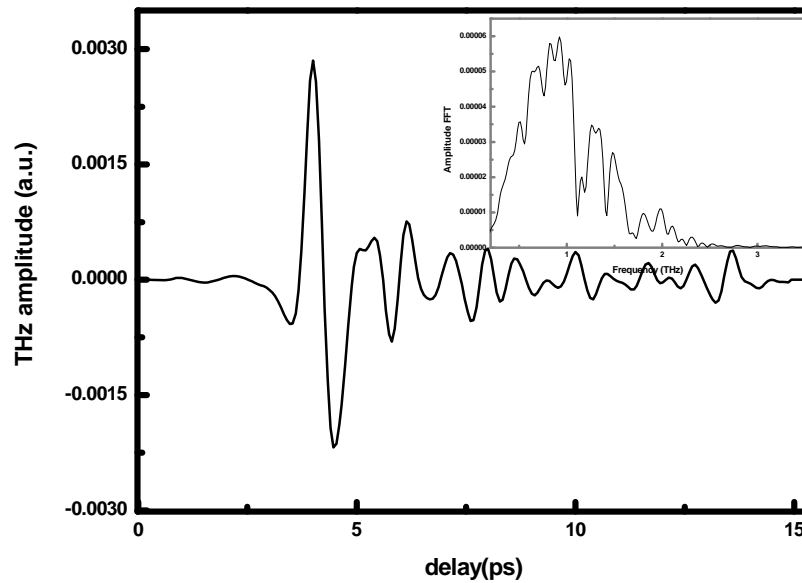
Figure 1-8 : The THz time domain waveform inset: its corresponding frequency domain
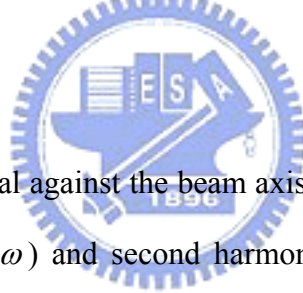
First, we rotate the BBO crystal against the beam axis which means varying the angle between fundamental beam (ω) and second harmonic beam (2ω). But during the experiment we found that there was terahertz which generated from the BBO crystal. By use of a teflon to block the laser beam behind BBO, we can measure the terahertz radiation from the BBO crystal, see Figure 1-9. The solid line is theoretically expected $\sin^4(\alpha)$ of the SHG efficiency. The terahertz generated from BBO was identified as optical rectification of fundamental beam. The terahertz radiation from BBO reach maximum when SHG efficiency is zero. Figure 1-10 show the terahertz signal generated by four wave mixing that is numerically subtracted the signal generated by BBO because the THz signal from BBO will overlap the signal from plasma. We can see that the maximum signal is at the angle $\pm 40°$ to the maximum SHG efficiency ($45°$ and $225°$)

18
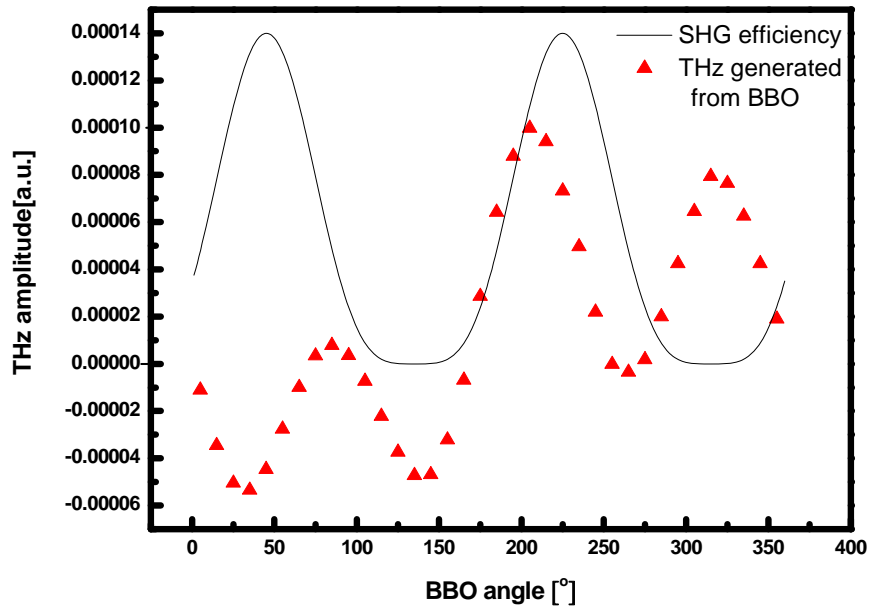
Figure 1-9 : Terahertz radiation from BBO versus its azimuthal angle
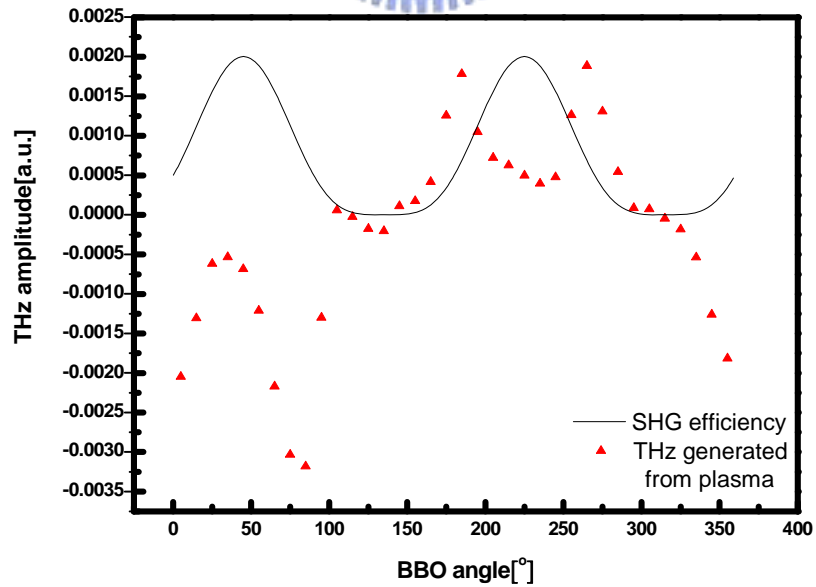
Figure 1-10 : Terahertz radiation from plasma versus the azimuthal angle of BBO

Four wave mixing predicts that the generated THz signal is proportional to the third order nonlinearity, electric field of second harmonic wave, the square of electric field of fundamental wave and their relative phase φ.

$$E_{THz} \propto \chi^{(3)} E_{2\omega} E_\omega^2 \sin(\varphi) \tag{22}$$

We can change the phase by varying the distance d between BBO and the focus point. The phase shift φ

$$\varphi = \frac{(2n_{2\omega} - n_\omega)\omega d}{c} \tag{23}$$

where $n_{2\omega}$ and n_ω are the refractive index of air at frequency ω and 2ω.

Figure 1-11 shows that terahertz amplitude is varied by adjusting the distance from BBO to focus point. The moving range only from 4.9 to $6.3\,cm$ is due to the damage threshold of BBO and its dimension area. The pump beam size is larger than BBO dimension area when the distance is larger than $6.4\,cm$, and close to the damage threshold of BBO crystal when the distance less than $4.9\,cm$.
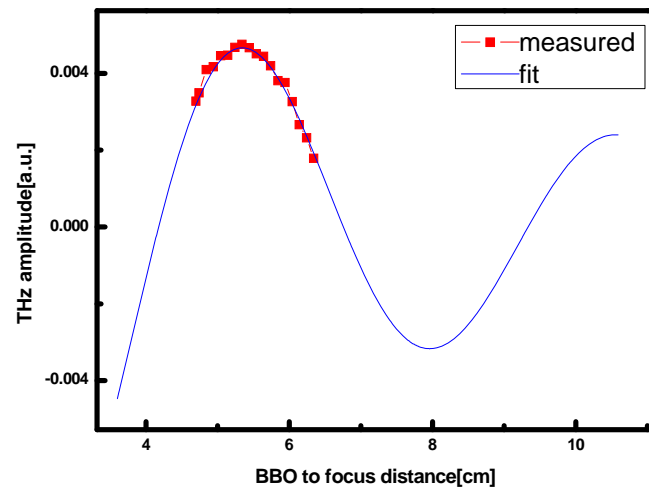
Figure 1-11 : THz amplitude versus the distance from BBO to focus point

The blue-solid line is the theoretical fitting. Changing the distance d is not only altering the relative phase but also changing the SHG efficiency and the beam spot size on the BBO crystal. The SHG power conversion efficiency [11] is defined as

$$\eta_{SHG} = \tanh^2(\frac{1}{2}\kappa A_1(0)z) \tag{24}$$

where $\kappa = \left(\frac{\omega}{n}\right)^{3/2}\sqrt{2\left(\frac{\mu_0}{\varepsilon_0}\right)}d$ is the phase mismatch. And we can derive that

$$E_{THz} \propto \sin(\varphi)\tanh(\frac{1}{d}) \tag{25}$$
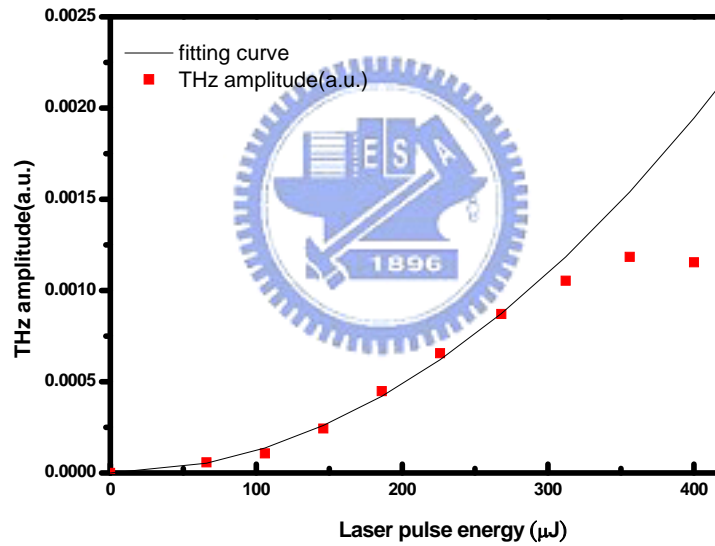
Figure 1-12 : THz amplitude versus laser pulse energy

We measured the THz signal intensity with varying the laser pulse energy before the BBO crystal, The results are shown in Figure 1-12, while the BBO angle was set at 185° and the distance $d = 4.7cm$.

Using the relation

$$E_{2\omega} \propto E_{\omega}^2 \propto I_{\omega} \tag{26}$$

Eq. (22) has quadratic dependence

$$E_{THz} \propto \chi^{(3)} I_{\omega}^2 \tag{27}$$

The pulse energy below $300\,\mu$J can be fitted well with Eq. (27), but the THz signal falls below the fitted quadratic curve in the higher pulse energies portion. It may be likely due to the defocusing of the laser beam by the plasma and reduces the effective peak intensity. In addition, at larger plasma volumes, phase mismatch and THz absorption effects are more likely to become significant. [12]

Reference

[1] http://www.advancedphotonix.com/ap_products/terahertz_whatis.asp

[2] A.Leitenstorfer, et al., Detectors and sources for ultrabroadband electro-optic sampling: Experiment and theory Applied Physics Letters 74, 1516-1518 (1999).

[3] Masahiko Tani, et al , Generation and detection of terahertz pulsed radiation with photoconductive antennas and its application to imaging, Meas. Sci. Technol. 13 (2002) 1739–1745

[4] Hamster H, Sullivan A, Gordon S, White W and Falcone R W, 1993 Phys. Rev. Lett. 71 2715

[5] Loffler T, Jacob F and Roskos H G 2000, Appl. Phys. Lett. 77 453

[6] You D, Jones R R and Bucksbaum P H 1993 Opt. Lett. 18 290

[7] Darrow J T, Zhang X-C and Auston D H 1992 IEEE J. Quantum Electron. 28 1607

[8] Auston D H, Cheung K P and Smith P R 1984 Picosecond photoconducting Hertzian dipoles Appl. Phys. Lett. 45 284–6

[9] Q. Wu and X.-C. Zhang, Free-space electro-optic sampling of terahertz beams

APL_vol67_p3523_1995

[10] D. J. Cook, Intense terahertz pulses by four-wave rectification in air, OL_25_1210_2000

[11] Photonics 6ed, Yariv and Yeh

[12] Markus Kress, Torsten Löff ler, Susanne Eden, Mark Thomson, and Hartmut G. Roskos, Terahertz-pulse generation by photoionization of air with laser pulses composed of both fundamental and second-harmonic waves, OPTICS LETTERS / Vol. 29, No. 10 / May 15, 2004
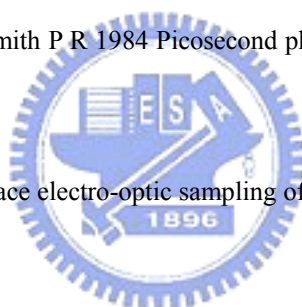
Chapter 2

Optical constant of ε-GaSe crystal in THz regime

2.1 Introduction to GaSe

2.1.1 GaSe properties

Gallium selenide (GaSe) is a semiconductor belongs to the III-VI layered semiconductor family like GaS and InSe, which has relatively large direct band gap of about $2.0\,eV$ at room temperature. There are four polytypes of GaSe (β-, γ-, δ- and ε-type) classed by the package type of separate layers and their amount in the unit cell. The methods of growing ε-GaSe crystal are mainly the Czochralski and Bridgman-Stockbarger methods. Gas transport reactions also yield the ε polytype with a large number of stacking faults. Needle crystals of γ, δ and ε polytypes are formed by vacuum sublimation.

Figure 2-1 shows the structure of ε-GaSe, and atomic configuration of ε-GaSe layers. The ε-GaSe consists of two layers and crystallizes with the space group D_{3h}^{1}, three anions form a tetrahedron along with the metal atom. The atoms are located in the planes normal to the *c*-axis in the sequence of Se–Ga–Ga–Se. Each layer consists of two planes of Ga atoms and surrounded by the unit planes of the Se atoms on two sides. Two sheets of the same layer are bonded with a mixture of covalent and ionic bonds, but the layers are hold by weak van der Waal's forces. Weakness of the interlayer binding of this single crystal gives rise to a strong anisotropy in the

electrical properties.
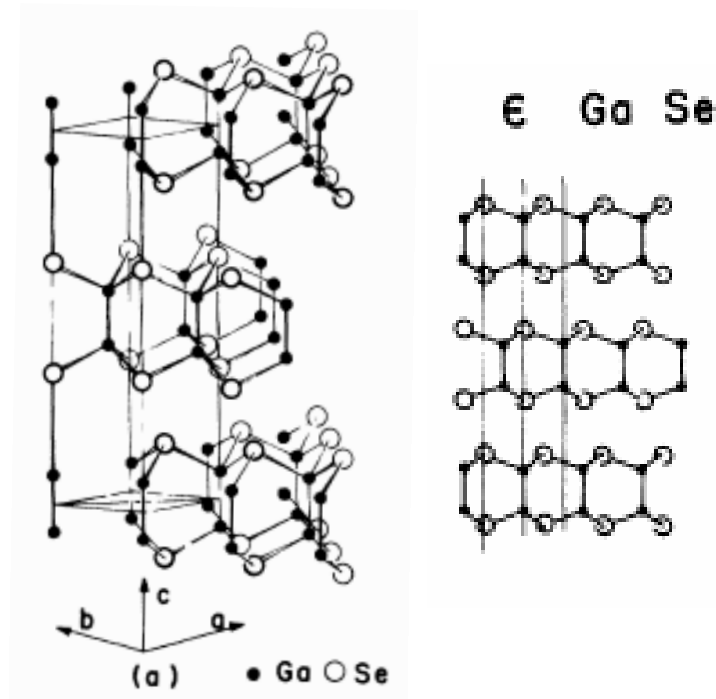
Figure 2-1 : The atomic configuration of ε-GaSe

It is highly transparent in the infrared region between the wavelengths $0.65 - 18$ μm, is also a promising candidate material for nonlinear optical conversion devices in the near- to far-infrared. Besides the removal of the constraint of the lattice mismatch, GaSe thin film has the advantages of stability to against heating and oxidation under the ultra high vacuum condition.

Due to its relatively large band gap energy of $2.0\,eV$, therefore impurity doping in GaSe has been investigated with a large amount of interest because of possible technical applications for photoelectric devices in the visible region. The electric and optical properties of GaSe doped with elements of groups I, II, IV, and VII have been reported by many researchers. [1]

For practical application of nonlinear optics, the crystals should have some properties.

25

Such as low scattering loss, large birefringence and nonlinear coefficient, wide transparency range, low absorption coefficient and mechanical strength. Few crystals have above properties, $LiNbO_3$, KDP, $AgGaSe_2$ are often used, Table 2-1 is the properties of these crystals [2].

Table 2-1 : Properties of some common used crystals, GaSe, $LiNbO_3$, KDP, $ZnGeP_2$, $AgGaSe_2$

Crystals	GaSe	$LiNbO_3$	KDP	$ZnGeP_2$	$AgGaSe_2$
Nonlinear coefficient (pm/V)	$d_{22} = 63$	$d_{33} = 25.2$	$d_{36} = 0.7$	$d_{36} = 70$	$d_{36} = 43$
Absorption coefficient (cm^{-1})	0.45	$0.0042 \parallel c$ $0.0028 \perp c$	$0.058 \perp c$ $0.006 \parallel c$	1.52	0.012-0.2
Refractive index n_o (at 1.064 μm) n_e	2.91 2.57	2.23 2.14	1.49 1.48	3.22 3.26	2.70 2.68
Transparency range (μm)	0.62~18	0.4~5.5	0.176~1.4	0.74~12	0.76~17

Among these nonlinear optical crystals, GaSe has a wide transparency range from a wavelength of 0.62 to 18 μm with low optical absorption coefficient lower than $1 cm^{-1}$. The ε-GaSe is a negative uniaxial crystal ($n_e < n_o$, n_o and n_e is the

refractive indices in the ordinary and extraordinary direction). It has high nonlinear optical coefficients among the top five birefringent crystals. Due to its large birefringence, it can satisfy phase matching (PM) conditions for optical configurations within the nonlinear optical crystals. Incoherent parametric generation tunable in the range of 3.5–18 μm in GaSe (type–I PM) was obtained by using actively mode-locked Er:YAG laser as a pump source[3]. Besides, there are a number of reports about using difference frequency generation (DFG) to achieve widely tunable and coherent mid-IR for GaSe. Recently, numerous papers reported on terahertz generation from GaSe, because it has lowest absorption coefficients in the THz wavelength region, see Figure 2-2.
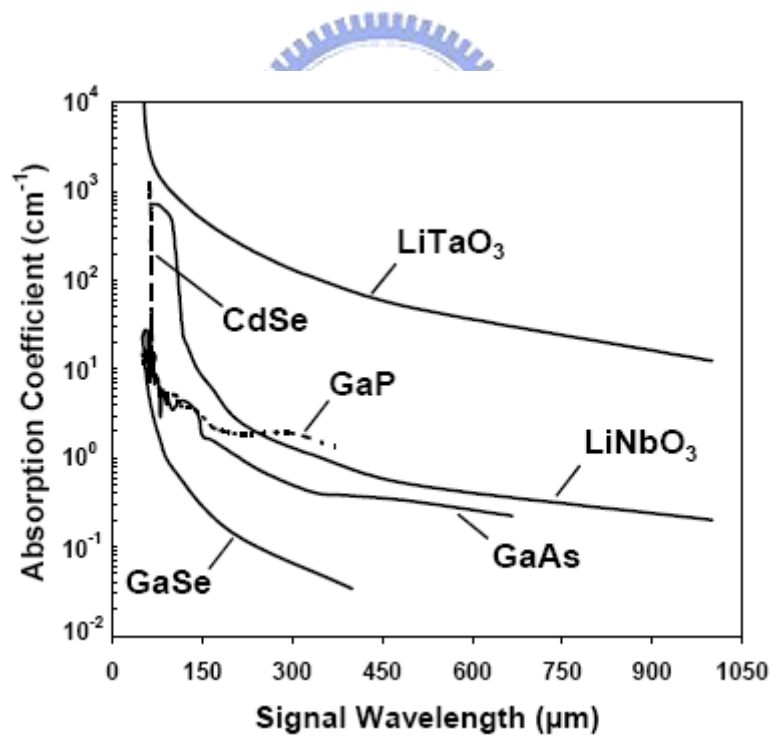
Figure 2-2 : Absorption spectra for e-ray in GaSe, CdSe, GaP, GaAs, $LiTaO_3$, $LiNbO_3$ based on

reference 4

27

Consequently, GaSe has the largest figure of merit ($d_{eff}^2/n^3\alpha^2$) for the THz generation, which is several orders of magnitude larger than that for bulk LiNbO$_3$ at 1 THz. An efficient and coherent high power THz wave tunable in the two extremely wide ranges of 2.7–38.4 and 58.2–3540 μm, with typical linewidths of 6000 MHz, has been achieved by Ding's group for the first time. [5]

2.1.2 The growth of GaSe

The GaSe crystals are grown and provided by Prof. Chen-Shiung Chang's group in NCTU. GaSe crystals were grown by a vertical Bridgman method, this method is good for growing single crystal ingots.

This method involves heating polycrystalline material in a container above its melting point and slowly cooling it from one end where a seed crystal is located. Single crystal material is progressively formed along the length of the container. The process can be carried out in a horizontal or vertical geometry.

It is a popular method of producing certain semiconductor crystals, such as gallium selenide and gallium arsenide where the Czochralski process is more difficult.
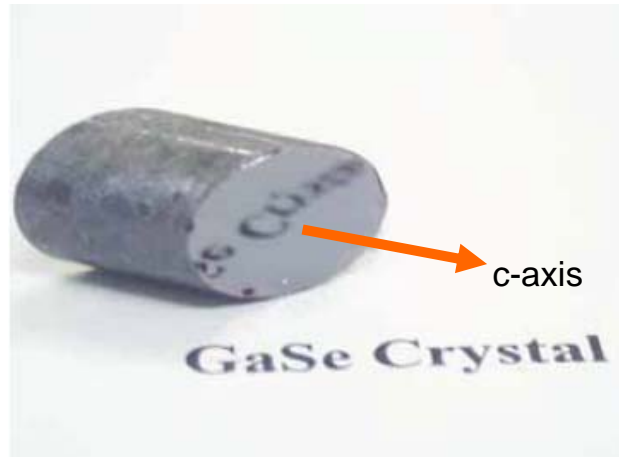
Figure 2-3 : The cleaved surface of GaSe

2.2　Analysis method

2.2.1　Analysis Method of Optical Constant from THz-TDS

As shown in Figure 2-4, the transmitted terahertz pulses propagate through the reference and sample. If the sample is thick enough, we can have a relatively clear separation in time between the main transmitted terahertz signal and the first refection signal which enable us to analyze the data on the main pulse only.
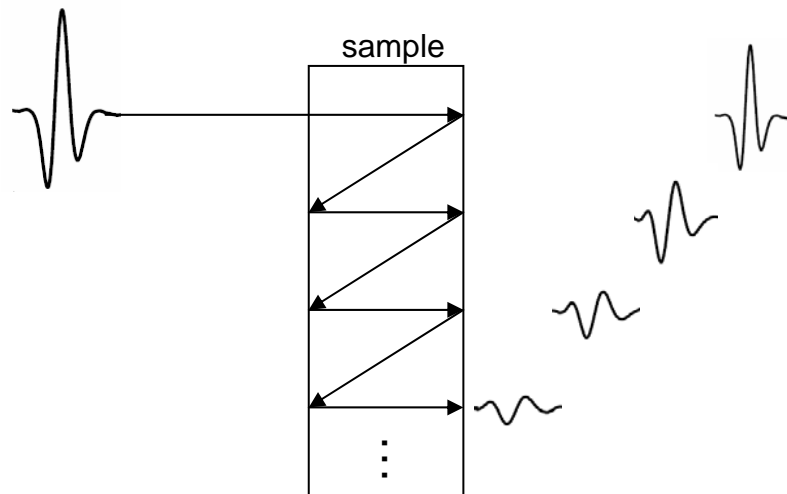
Figure 2-4 : Schematic of multi-reflection structure of sample

$$\frac{\widetilde{E}_s(\omega)}{\widetilde{E}_r(\omega)} \equiv \sqrt{P_s(\nu,d)/P_r(\nu,d)} \exp(i\phi(\omega))$$

$$= \tilde{t}_{as}\tilde{t}_{sa} \exp(i\frac{(\tilde{n}-1)\omega d}{c})$$

where $\widetilde{E}_r(\omega)$ and $\widetilde{E}_s(\omega)$ are Fourier transform of $E_r(t)$ and $E_s(t)$, respectively. $P_s(\nu,d)$ and $P_r(\nu,d)$ are the power transmittance for sample and reference. $\tilde{n} = n - i\kappa$ is the complex refractive index.

The refractive index n(ν) can be determined by the phase difference:

$$n(\nu) = 1 + c\Delta\phi/2\pi\nu d \tag{1}$$

and the absorption coefficient can be calculated by the transmittance:

$$\alpha(\nu) = -(1/d)\ln[\eta \cdot P_s(\nu,d)/P_r(\nu,d)] \tag{2}$$

η is the Fresnel reflection loss correcting factor due to the two sample/air interfaces. These approximation experiments enabled the quite accurate determination of the refraction index $n(\nu)$ and absorption coefficient $\alpha(\nu)$ of the sample crystal.

To analyze experimental data, one usually takes a model dielectric function which is the combination of one Drude peak and various Lorentz oscillators. Drude model can describe the free-carriers, and bound carriers can be described from the Lorentz model. Using the Drude-Lorentz model for the dielectric response analysis, we can extract parameters from the THz-TDS measured data, such as plasma frequency ω_p, the average momentum relaxation time $\langle\tau\rangle$, and the mobility μ. The theoretical treatment is as follows:

The total complex dielectric function, consisted of bound electrons, optical phonons,

and conduction band electrons in the terahertz region is given by [6]:

$$\varepsilon(\omega) = (n - i\kappa)^2$$

$$= \varepsilon(\infty) + \sum_{j=1}^{J} \frac{S_j \omega_{TO_j}^2}{\omega_{TO_j}^2 - \omega^2 - i\Gamma_j\omega} - \frac{\omega_p^2}{\omega(\omega + \frac{i}{\langle\tau\rangle})} \tag{3}$$

where the summation is over the lattice oscillators with the strength S_j; the resonance transverse optical phonon ω_{TO_j}; the phonon relaxation rate Γ_j, and the average momentum relaxation time for carrier $\langle\tau\rangle$. The static dielectric constant is $\varepsilon_{dc} = \varepsilon_\infty + \sum_j S_j$, ε_∞ denotes the valance electron contribution to the high frequency dielectric function.

From the Drude model approximation [6], the complex conductivity can be expressed as follows:

$$\varepsilon(\omega) = (n - i\kappa)^2 = \varepsilon(\infty) + \frac{i\hat{\sigma}}{\omega\varepsilon_0} \tag{4}$$

The complex conductivity can be presented as follows:

$$\hat{\sigma}(\omega) = \sigma_r(\omega) + i\sigma_i(\omega) \tag{5}$$

Substituting Eq. (5) to Eq. (4), the real part and imaginary part of the conductivity can be derived as follows:

$$\sigma_r(\omega) = 2n\kappa\omega\varepsilon_0 \tag{6}$$

$$\sigma_i(\omega) = \varepsilon_0\omega(\varepsilon(\infty) - n^2 + \kappa^2) \tag{7}$$

From Eq. (3) and Eq. (4), the complex conductivity can be described as follows:

$$\hat{\sigma}(\omega) = \sigma_r(\omega) + i\sigma_i(\omega)$$

$$= \frac{i\varepsilon_0\omega_p^2}{\omega + i\langle\tau\rangle^{-1}} - i\omega\varepsilon_0 \sum_{j=1}^{J} \frac{S_j\omega_{TO_j}^2}{\omega_{TO_j}^2 - \omega^2 - i\Gamma_j\omega}$$

(8)

The phonon resonance effect is also considered in Eq. (8). The measured real and imaginary part of the complex conductivity can be theoretical fitted by the following parameters: plasma frequency; the average momentum relaxation time, and the optical phonon frequency.

Furthermore, with average momentum relaxation time, we can calculate mobility can be expressed as follows:

$$\mu = \frac{e\langle\tau\rangle}{m^*}$$

(9)
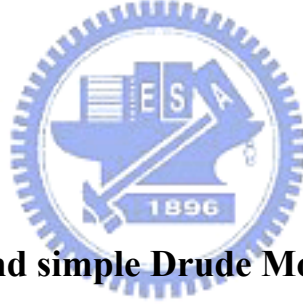
2.2.2 Lorentz Model and simple Drude Model

Lorentz model

The simplest model to describe the response of the medium to an electromagnetic field is the Lorentz model. In that model we consider an electron of mass m with charge e which bound to the nucleus in a similar way a small mass can be bounded to a large one:

$$m\frac{d^2\vec{r}(t)}{dt^2} + m\Gamma\frac{d\vec{r}(t)}{dt} + m\omega_0\vec{r}(t) = -e\vec{E}(t)$$

(10)

To solve the differential equation, first, we can take Fourier transform of Eq. (10)

$$\left(-m\omega^2 - i\omega m\Gamma + m\omega_0^2\right)\vec{r}(\omega) = -e\vec{E}(\omega)$$

(11)

Then we can get

$$\bar{r}(\omega) = \frac{-e\bar{E}(\omega)}{m(\omega_0^2 - \omega^2 - i\Gamma\omega)} \qquad (12)$$

The induced dipole moment is defined as

$$\vec{p}(\omega) = -e\vec{r}(\omega) \qquad (13)$$

If there are N atoms in the unit volume, then the net dipole moment per unit volume is:

$$\vec{P}(\omega) = \frac{1}{V}\sum_i^{NV} \vec{p}_i(\omega) = N\langle \vec{p}(\omega) \rangle \qquad (14)$$

$$\chi(\omega) = \frac{P(\omega)}{\varepsilon_0 E(\omega)} = \frac{Ne^2}{\varepsilon_0 m} \frac{1}{\omega_0^2 - \omega^2 - i\Gamma\omega}$$
$$= \frac{\omega_p^2}{\omega_0^2 - \omega^2 - i\Gamma\omega} \qquad (15)$$

Here we set plasma frequency

$$\omega_p = \sqrt{\frac{Ne^2}{\varepsilon_0 m}} \qquad (16)$$

The dielectric function is

$$\varepsilon(\omega) = 1 + \frac{\omega_p^2}{\omega_0^2 - \omega^2 - i\Gamma\omega} \qquad (17)$$

Simple Drude model

If we set $\omega_0 = 0$, means that no electrons are bounded , i.e. free electron, Eq. (10) becomes

$$m\frac{d^2\vec{r}(t)}{dt^2} + m\Gamma\frac{d\vec{r}(t)}{dt} = -e\vec{E}(t) \qquad (18)$$

This is the well known Drude model used to describe the low frequency response of metals.

The solution of Eq. (18) is

$$\bar{r}(\omega) = \frac{e\overline{E}(\omega)}{m(\omega^2 + i\Gamma\omega)} \tag{19}$$

$$\chi(\omega) = -\frac{\omega_p^2}{\omega^2 + i\Gamma\omega} \tag{20}$$

The current density is

$$\overline{J} = Ne\langle v \rangle = \sigma\overline{E} \tag{21}$$

The complex conductivity can then be derive

$$\hat{\sigma}(\omega) = \frac{Ne^2}{m}\frac{i\omega}{\omega^2 + i\omega\Gamma} = \frac{i\varepsilon_0\omega_p^2}{\omega + i\langle\tau\rangle^{-1}} \tag{22}$$

2.3 Experimental setup

We use mode-locked femtosecond Ti:sapphire laser (Spectra Physics Tsunami) as our light source. Figure 2-5 is the schematic of setup. The laser output is split into two beams, one is the pump beam; another one is the probe beam. The pump beam is focused on the emitter by an objective lens, a low-temperature grown Gallium arsenide (LT-GaAs) photoconductive dipole antenna is utilized. The generated THz pulses are collimated by gold-coated parabolic mirrors onto the sample. The transmitted pulses from the sample are focused by another parabolic gold mirror onto the THz detector, which is also a photoconductive antenna. The Ti:sapphire laser probe pulse that impinged on the LT-GaAs generates charge carriers and effectively turns the antenna on for a short time interval. The electrical signal of antenna detector is connected to a lock-in amplifier in order to increase the signal/noise ratio (SNR).
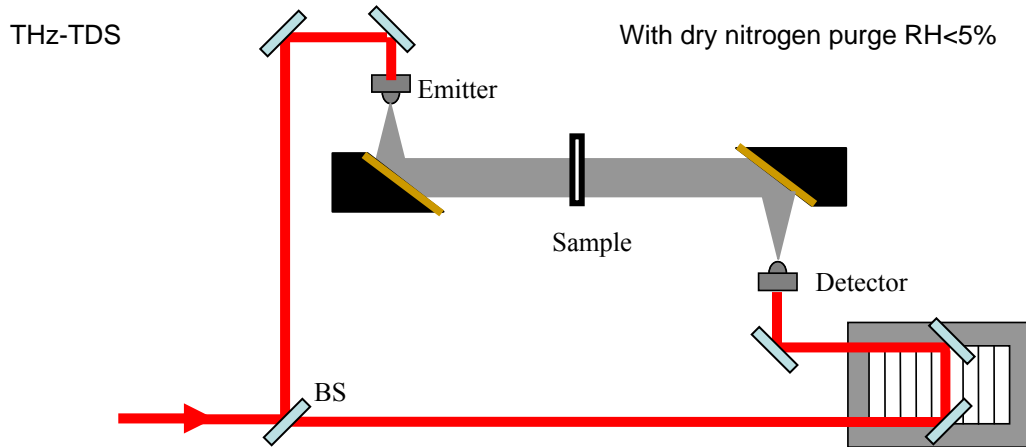
Figure 2-5 : The experimental setup of the PC antenna based THz-TDS

2.4 Experimental Results

2.4.1 Raman spectroscopy

The Raman scattering measurements were performed by a Jobin-Yvon U1000 Raman system [7]. The Raman spectra were excited by using the 514.5 nm line from an Argon-ion laser with a notch filter to filter out the Rayleigh scattering of the laser. Raman signals were collected by the double-grating spectrometer and detected by a LN_2 cooled charge coupled device (CCD).
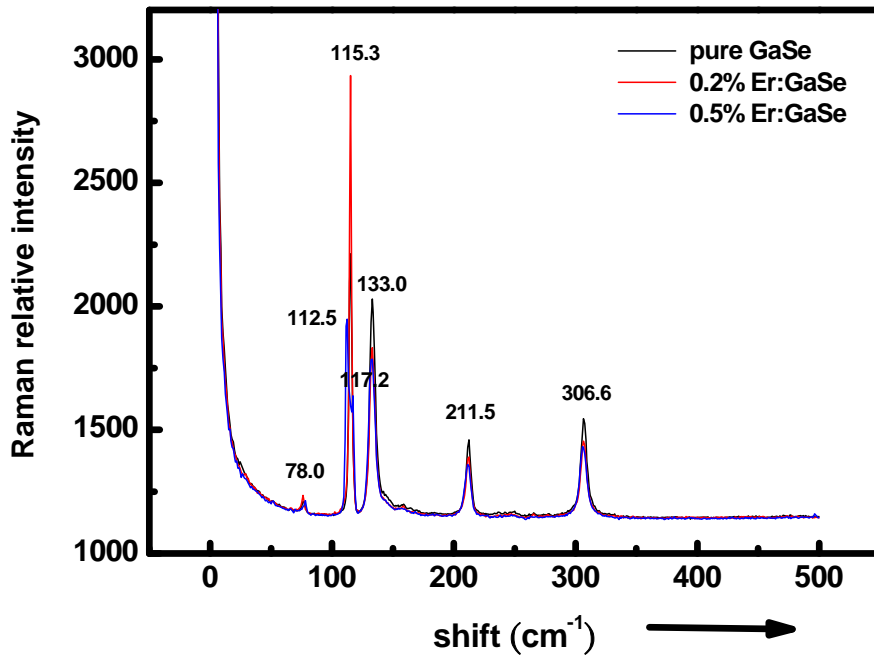
Figure 2-6 : Raman spectra of pure GaSe, 0.2% Er:GaSe, 0.5% Er:GaSe

The measured Raman spectra data are showed in Figure 2-6. There are phonon frequencies at $78\,cm^{-1}$, $115.3\,cm^{-1}$, $133.0\,cm^{-1}$, $211.5\,cm^{-1}$, $306.6\,cm^{-1}$, for pure GaSe, 0.2% Er:GaSe and 0.5% Er:GaSe. These are coincidence with the report [1], except $78\,cm^{-1}$. The low frequency band $19\,cm^{-1}$, $60\,cm^{-1}$ in reference 1 were not observed because of the noise background of laser. At $115.3\,cm^{-1}$, 0.2% Er:GaSe has higher Raman intensity, it may be due to the better crystalline. The splitting peaks at $112.5\,cm^{-1}$ and $117.2\,cm^{-1}$ for 0.5% Er:GaSe, it may be likely due to the defects in the crystal.

2.4.2 Optical Constants in THz Region

One of the reference THz waveform is shown in Figure 2-7. The nitrogen is

continuously infusing to THz-TDS system to reduce water vapor absorption of THz radiation. The inset of Figure 2-7 is the frequency spectrum of the measured THz radiation. The signal to noise ratio (SNR) is about 1000000:1, and the absorption lines of water vapor at 0.557, 0.752, 0.988, 1.097, 1.113, 1.163, 1.208, 1.229 and 1.411 THz [7] are not existed.

We prepare two kinds of samples, pure GaSe and 0.2% Er:GaSe. The thickness of pure GaSe is about 669 μm, 0.2% Er:GaSe is about 663 μm.
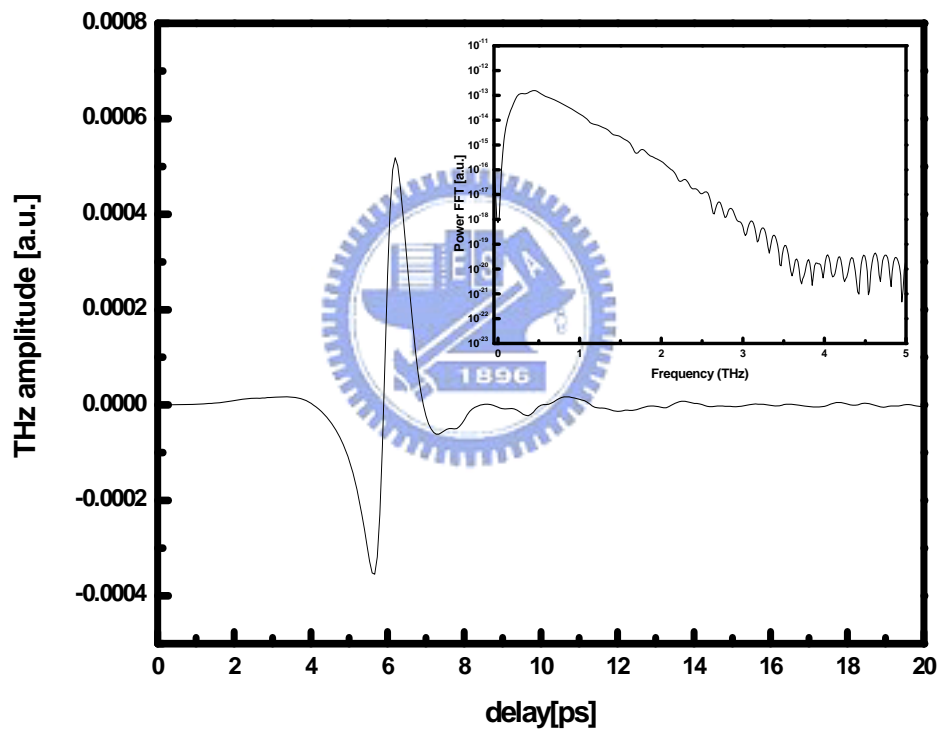

Figure 2-7 : The terahertz time domain waveform. Inset: The corresponding frequency spectrum

All the data are performed on the main pulse. Using the method in chapter 2.2.2, the real and imaginary parts of refractive index are shown in Figure 2-8 and Figure 2-9. The refractive index is approximately 3.2. A strong absorption peak is clearly

indicated at 0.589 THz. It can be attributed to an interlayer vibration of GaSe with E'-type symmetry. The presence of the low-frequency sharp peak of "rigid layer mode" at 19 cm⁻¹ indicates the pure GaSe crystal to be in ε-phase. It is also clearly shown in the absorption spectrum, see Figure 2-10. The absorption coefficient of pure GaSe is below $10\,cm^{-1}$ from 0.2 to 1 THz. For 0.2% Er:GaSe, the average absorption coefficient is $55\,cm^{-1}$ from 0.2 to 1 THz.

Using Lorentz-Drude model we can extract some parameters from the complex conductivity, such as plasma frequency; the average momentum relaxation time and the optical phonon frequency. The real part of conductivity of pure GaSe and 0.2% Er:GaSe is shown in Figure 2-11.

The measured and theoretical fitting of the imaginary part of complex conductivity is shown in Figure 2-12 and Figure 2-13.
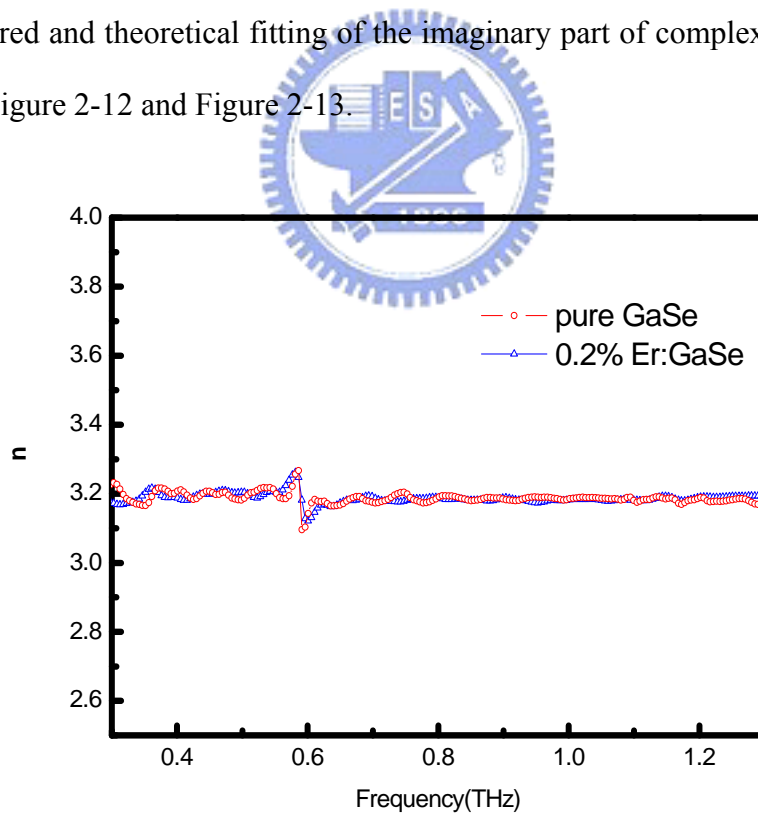

Figure 2-8 : The real part of refractive index of pure GaSe and 0.2% Er:GaSe
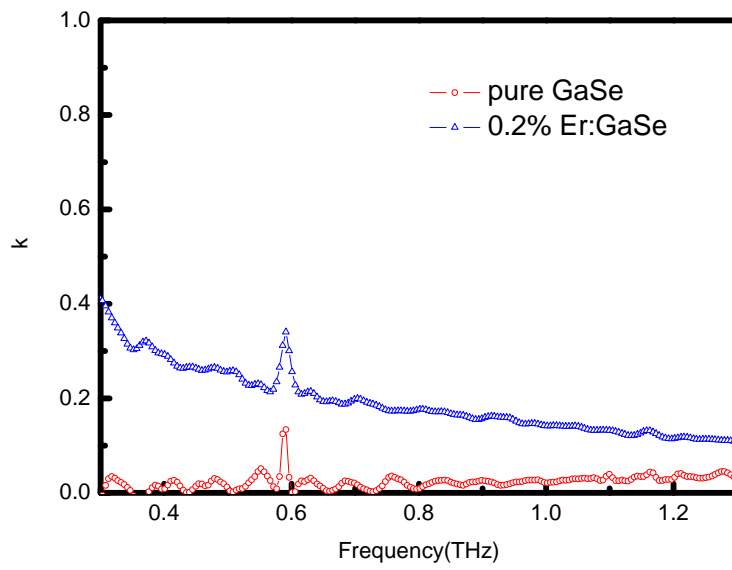
Figure 2-9 : The imaginary part of refractive index of pure GaSe and 0.2% Er:GaSe
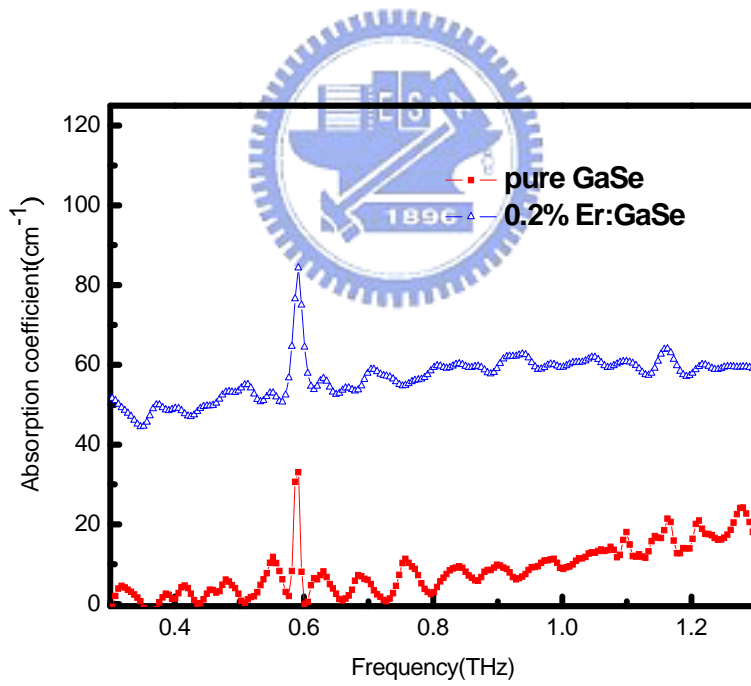
Figure 2-10 : The absorption coefficient of pure GaSe and 0.2% Er:GaSe
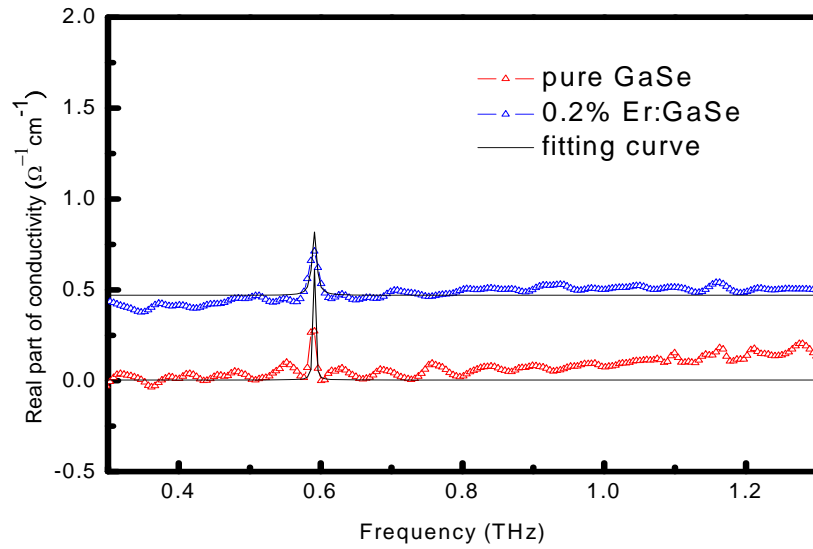
Figure 2-11 : The real part of conductivity of pure GaSe and 0.2% Er:GaSe

The measured real and imaginary part of the complex conductivity can be theoretical fitted by the following parameters: plasma frequency; the average momentum relaxation time, and the optical phonon frequency. The parameters obtained from fitting the measured experimental data are listed in Table 2-1.

Table 2-2 : Fitting parameters

	Pure GaSe	0.2% Er:GaSe
Phonon frequency ω_{TO}	0.589 THz	0.589 THz
Plasma frequency ω_P	1.5 THz	22.05THz
Momentum relaxation time $<\tau>$	23 fs	10 fs
Phonon	0.003 THz	0.0075 THz

relaxation rate Γ_j		
Oscillator strength S_j	0.06	0.085
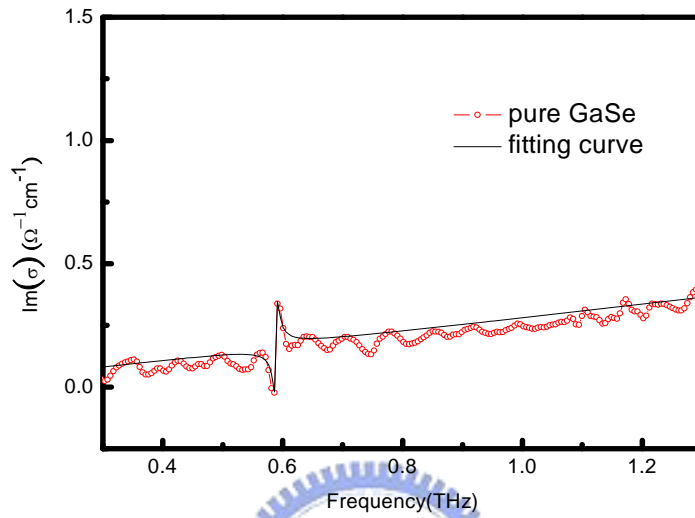
Figure 2-12 : The imaginary part of conductivity of pure GaSe and its theoretical fitting
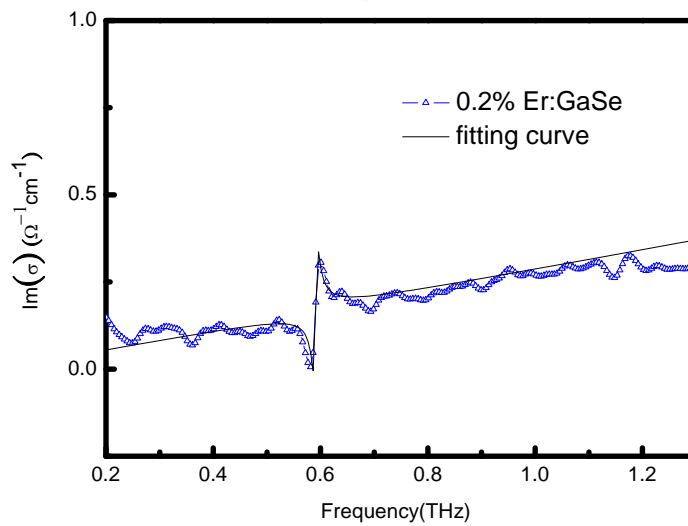
Figure 2-13 : The imaginary part of conductivity of 0.2% Er:GaSe and its theoretical fitting

The mobility can be calculated by Eq. (9) where effective mass m*=0.73 m_0 [10] and

$m_0 = 9.1 \times 10^{-31} kg$. Therefore, the mobility of the pure GaSe is derived as $\mu = 81 cm^2/Vs$, for 0.2% Er:GaSe $\mu = 39 cm^2/Vs$. The mobility measured by Hall measurement is $\mu = 56.76 cm^2/Vs$ and $\mu = 34.073 cm^2/Vs$. [8]

Reference

[1] K. Allakhverdiev et.al , "Lattice vibrations of pure and doped GaSe, Materials", Research Bulletin 41 (2006) 751–763

[2] David N. Nikogosyan, "Nonlinear Optical Crystals: A Complete Survey", Springer

[3] K. L. Vodopyanov et.al, "High efficiency middle IR parametric superradiance in $ZnGeP_2$ and GaSe crystals pumped by an erbium laser", Opt. Commun. 83, 322 (1991).

[4] E. D. Palik, Handbook of Optical Constants of Solids, Academic, NY, Vol. I (1985);Vol. II (1991); and Vol. III (1998).

[5] Wei Shi and Yujie J. Ding, "A monochromatic and high-power terahertz source tunable in the ranges of 2.7–38.4 and 58.2–3540 mm for variety of potential applications", APL 84 1635 2004

[6] B. L. Yu, F. Zeng, V. Kartazayev, and R. R. Alfano, "Terahertz studies of the dielectric response and second-order phonons in a GaSe crystal", Appl. Phys. Lett. 87, 182104 (2005).

[7] http://rdweb.adm.nctu.edu.tw/page.php?serial=344

[8] Martin van Exter, Ch. Fattinger, and D. Grischkowsky "Terahertz time-domain spectroscopy of water vapor", Opt. Lett. Vol. 14, No. 20 1989

[9] Yu-Kuei Hsu and Chen-Shiung Chang, "Electrical properties of GaSe doped with Er", JAP, 96, 1563 (2002).

[10] A.Mercier,,PRB_11_2243_1975

Chapter 3

Study of Optical Parametric Amplification in Terahertz

3.1   Introduction to Optical Parametric Amplification

The field of nonlinear optics was initiated shortly after the demonstration of the laser with the experiment of second harmonic generation by Franken and colleagues in 1961. Due to the increase of power spectral brightness, the nonlinear experiment were possible be achieved.

Optical parametric amplifier (OPA) is one of second order nonlinear process. The process of OPA is similar to difference frequency generation (DFG), only differs from the initial conditions, the signal beam is much weaker than pump beam, after the interaction the signal beam can get significant amplification.

The second order nonlinear interaction is characterized by the generation of a nonlinear polarization

$$\overrightarrow{P}_p(\omega_p) = \varepsilon_0 \overleftrightarrow{\chi}(-\omega_p, \omega_s, \omega_i) : \overrightarrow{E}_p(\omega_p)\overrightarrow{E}_s(\omega_s) \tag{1}$$

where $\overrightarrow{P}_p(\omega_p)$ is the nonlinear polarization at frequency ω_p, ε_0 is the dielectric constant, $\overleftrightarrow{\chi}(-\omega_p, \omega_s, \omega_i)$ is the nonlinear susceptibility, $\overrightarrow{E}_p(\omega_p)$ and $\overrightarrow{E}_s(\omega_s)$ are the interacting fields.

Commonly, the geometries of OPA including the collinear and non-collinear

geometries, due to the different geometry, the two configurations have the different applications and characteristics. For example, collinear OPA has wider tuning range, non collinear OPA has broader bandwidth.
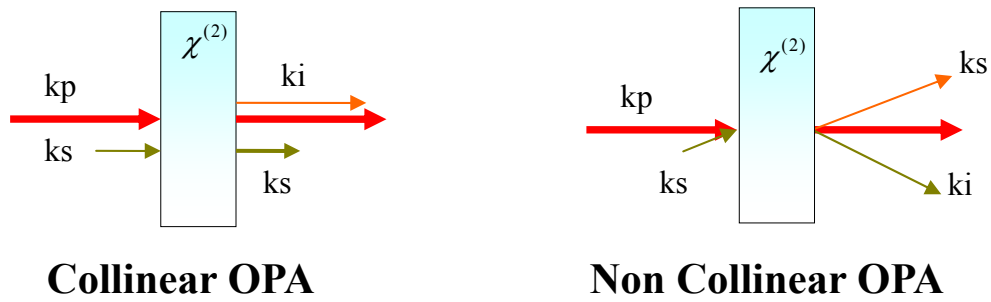
Figure 3-1 : Geometries of OPA

Consider three beams propagate and interact in a nonlinear medium, pump beam, signal beam, idler beam, at frequency ω_p, ω_s and ω_i, respectively.

In the interaction, the energy conservation should be satisfied.

$$\hbar\omega_p = \hbar\omega_s + \hbar\omega_i \qquad (2)$$

At the same time, to make more efficient interaction, the momentum conservation (or phase matching condition) must be satisfied

$$\vec{k}_p = \vec{k}_s + \vec{k}_i . \qquad (3)$$

where $\vec{k}_p$, $\vec{k}_s$ and $\vec{k}_i$ are the wave vectors of pump, signal and idler beam, respectively. This process leads to an increase in the signal photon flux and therefore the signal beam is amplified.

According to the polarization of the three interacted beams, OPA can be classified by

two types, type-I and type-II OPA. If both signal beam and idler beam have the same

polarization and perpendicular to the polarization of the pump beam, that is type-I

phase matching. If only one of the two beams have the same polarization with the

pump beam, that is type-II phase matching. [5]

3.2 Theory of OPA

3.2.1 Coupled wave Equations

Started from Maxwell's equations

$$\vec{\nabla} \cdot \vec{D} = 0$$

$$\vec{\nabla} \times \vec{E} = -\frac{\partial \vec{B}}{\partial t} \tag{4}$$

$$\tag{5}$$

$$\vec{\nabla} \cdot \vec{B} = 0 \tag{6}$$

$$\vec{\nabla} \times \vec{H} = \vec{J} + \frac{\partial \vec{D}}{\partial t} \tag{7}$$

and the constitutive equations

$$\vec{D} = \varepsilon_0 \varepsilon_r \vec{E} + \vec{P} \tag{8}$$

$$\vec{B} = \mu \vec{H} \tag{9}$$

$$\vec{\nabla} \times \vec{\nabla} \times \vec{E} = -\mu_0 \frac{\partial}{\partial t} \vec{\nabla} \times \vec{H}$$

$$= -\mu_0 \frac{\partial}{\partial t} \sigma \vec{E} - \mu_0 \frac{\partial^2}{\partial t^2} \varepsilon \vec{E} - \mu_0 \frac{\partial^2}{\partial t^2} \overline{P_{NL}} \tag{10}$$

Assume the medium is magnetically inactivity and monochromatic plane wave

propagating in the near field in z-direction.

Eq. (10) becomes

$$\frac{\partial^2 E}{\partial z^2} - \mu_0 \sigma \frac{\partial E}{\partial t} - \mu_0 \varepsilon \frac{\partial^2 E}{\partial t^2} = \mu_0 \frac{\partial^2 P}{\partial t^2} \tag{11}$$

With $\quad E_i(z,t) = \sum_m \mathrm{Re}(E_{im} \exp j(\omega_m t - k_m z))$, $\tag{12}$

$$P_i(z,t) = \sum_m \mathrm{Re}(P_{im} \exp j(\omega_m t - k_m z)) \tag{13}$$

where $i = x \text{ or } y$ represents the direction of polarization, $m = p \text{ or } s \text{ or } i$ the beam of interaction. Substitute Eq. (12) and (13) into Eq. (10) and apply slowly-varying-amplitude approximation (SVA)

$$(\frac{d^2 E}{dz^2}) \ll 2k(\frac{dE}{dz}) \tag{14}$$

We can derive

$$\frac{\partial E_m}{\partial z} = -j \frac{\mu_0 c \omega_m}{2 n_m} P_m \tag{15}$$

The nonlinear polarization components with envelope representation are

$$P_s = 2\varepsilon_0 d_{eff} E_i^* E_p e^{-j\Delta kz} \tag{16a}$$

$$P_i = 2\varepsilon_0 d_{eff} E_s^* E_p e^{-j\Delta kz} \tag{16b}$$

$$P_p = 2\varepsilon_0 d_{eff} E_s E_i e^{+j\Delta kz} \tag{16c}$$

$$\Delta \vec{k} = \vec{k}_p - \vec{k}_s - \vec{k}_i$$

d_{eff} is called effective nonlinear optical coefficient, depending on the propagation direction and polarization of the beam.

Substituting Eq. (16a), (16b), (16c) into Eq. (15)

$$\frac{\partial E_s}{\partial z} = -j\frac{\omega_s d_{eff}}{n_s c} E_i^* E_p e^{-j\Delta kz} \tag{17a}$$

$$\frac{\partial E_i}{\partial z} = -j\frac{\omega_i d_{eff}}{n_i c} E_s^* E_p e^{-j\Delta kz} \tag{17b}$$

$$\frac{\partial E_p}{\partial z} = -j\frac{\omega_p d_{eff}}{n_p c} E_s E_i e^{+j\Delta kz} \tag{17c}$$

Eq. (17) can describe second order nonlinear phenomena, such as second harmonic generation (SHG), difference frequency generation (DFG), optical parametric amplification (OPA). By some manipulations, Eq. (17) can be cast into the form called Manley-Rowe relations, Eq. (18).

$$\frac{1}{\omega_i}\frac{dI_i}{dz} = \frac{1}{\omega_s}\frac{dI_s}{dz} = -\frac{1}{\omega_p}\frac{dI_p}{dz} \tag{18}$$

where $I_j = \frac{1}{2}\varepsilon_0 c M_j |E_j|^2$

3.2.2   Pump non-depletion condition

In a strong pumping field, the photon of signal beam stimulates the generation of additional the photon at signal wavelength and the photon at idler wavelength. Similarly, the generation of idler beam stimulates the generation of signal photon. Therefore, it will reinforce the generation of the photon of idler and vice versa, giving a positive feedback.

Consider the condition pump non-depletion, with initial conditions $E_p \cong constant$, initial signal beam amplitude E_{s0} and no idler beam generated $E_{i0} = 0$

We can solve Eq. (17) to get the signal and idler beam intensity after pass through a

nonlinear optical crystal with length L.

$$I_s(L) = I_{s0}[1 + \frac{\Gamma^2}{g^2}\sinh^2(gL)],$$ (19a)

$$I_i(L) = I_{s0}\frac{\omega_i}{\omega_s}\frac{\Gamma^2}{g^2}\sinh^2(gL),$$ (19b)

where

$$g = \sqrt{\Gamma^2 - (\frac{\Delta k}{2})^2}$$ (20)

$$\Gamma^2 = \frac{\omega_i\omega_s d_{eff}^2 |E_p|^2}{n_i n_s c^2} = \frac{2\omega_i\omega_s d_{eff}^2 I_p}{n_i n_s n_p \varepsilon_0 c^3} = \frac{8\pi^2 d_{eff}^2 I_p}{n_i n_s n_p \lambda_i \lambda_s \varepsilon_0 c}$$ (21)

3.2.3 Pump depletion Condition

Consider pump depletion condition, under perfect phase matching $\Delta k = 0$. After several steps of basis transformation and the change of variables, Eq. (17) can be rewritten as the form of Jacobi's elliptic function:[4]

$$I_s(r) = I_s(0) + \frac{\omega_s}{\omega_p}I_p(0)(1 - sn^2[\frac{r - r_0}{l}, \gamma]) = I_s(0) + \frac{\omega_s}{\omega_p}I_p(0)(1 - sn^2[\frac{r\Gamma}{\gamma} - K(\gamma), \gamma])$$ (22)

$$I_i(r) = \frac{\omega_i}{\omega_p}I_p(0)(1 - sn^2[\frac{r - r_0}{l}, \gamma]) = \frac{\omega_i}{\omega_p}I_p(0)(1 - sn^2[\frac{r\Gamma}{\gamma} - K(\gamma), \gamma])$$ (23)

$$I_p(r) = I_p(0)(1 - sn^2[\frac{r - r_0}{l}, \gamma]) = I_p(0)(1 - sn^2[\frac{r\Gamma}{\gamma} - K(\gamma), \gamma])$$ (24)

where $\dfrac{1}{l} = \dfrac{\pi d_{eff}\left[8I_p(0)\right]^{1/2}}{(\varepsilon_0 n_s n_i n_p \lambda_s \lambda_i c)^{1/2}}(1 + I_s(0)\omega_p \big/ \left[I_p(0)\omega_s\right])^{1/2} = \dfrac{\Gamma}{\gamma}$ (25)

and $\dfrac{r_0}{l} = K(\gamma) = \dfrac{1}{2}\ln\left(16\left[1 + \dfrac{I_p(0)\omega_s}{I_s(0)\omega_p}\right]\right)$ (26)

49

$$K(\gamma) = \frac{1}{4} \int_{-\pi}^{\pi} \frac{\mathrm{d}\theta}{\sqrt{1-\gamma^2 \sin^2(\theta)}}$$, is the complete elliptical function of the first kind.

$$\gamma^2 = \frac{1}{1 + \dfrac{I_s(0)\omega_p}{I_p(0)\omega_s}}$$, the ratio of the number of photons in the input pump beam to the

total input photon number.

3.2.4   Group velocity Mismatch

When ultrafast pulses with different optical frequencies propagate in the medium, their group velocities will in general be different. Two pulses are overlapping in the beginning, after some propagation distance they no longer overlap.

As the pulse enters the crystal:
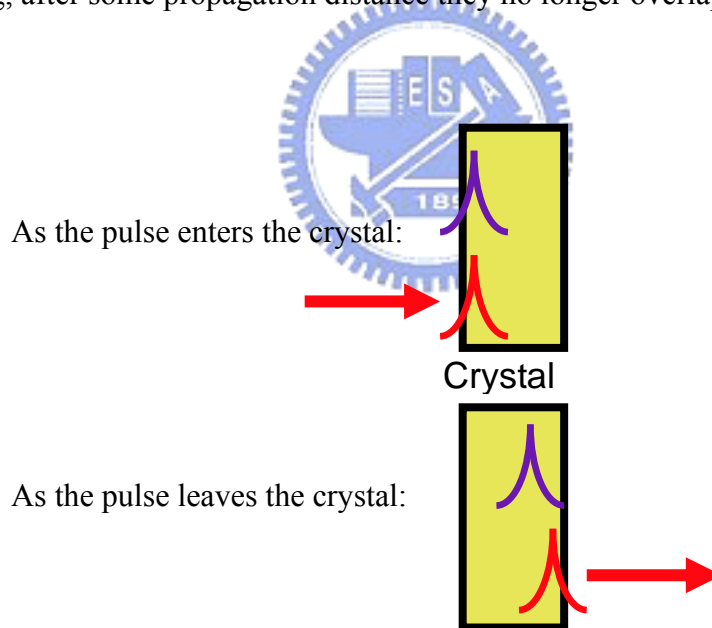
Crystal

As the pulse leaves the crystal:

Figure 3-2 : Schematics of group velocity mismatch of ultrashort optical pulse in the medium

This is called temporal walk-off, and group velocity mismatch limits the effective interaction length.

Quantitatively, the group velocity mismatch is defined as the difference of the inverse group velocities

$$\delta_{jp} = 1/v_{gj} - 1/v_{gp} \tag{27}$$

It has the unit s/m, generally in ultrafast regime the unit is fs/mm or ps/mm.

If the crystal length is shorter than the temporal walk-off length, GVM can be neglected. If the crystal length is comparable or longer than the walk-off length, we should take account of GVM effect. There is a significant difference between the cases which δ_{sp} and δ_{ip} have the same or different signs.

(1) $\delta_{sp}\delta_{ip} > 0$

Both the signal and the idler are away from the pump beam in the same direction, so the parametric interaction of the signal/idler and the pump beam disappear for the propagation distance longer than the quasi-static interaction length. This phenomenon can be proven by numerical solving the differential equation. Its solution show that when the crystal length is longer than the quasi-static interaction length, the signal can not increase and eventually saturates.

(2) $\delta_{sp}\delta_{ip} < 0$

In this case, the signal and the idler move in the opposite direction with respect to the pump beam. It seems that the two pulses stay localized under the pump pulse, so the gain continuously increases as the crystal length increases. Its thought is that the signal slightly moves to the left of the pump; in the parametric process, the signal generates the idler and the idler moves to the right through the peak of the pump beam. Then, the idler also generates the signal, and the signal moves to the left toward the peak of the pump beam. So, in this regime, increasing the crystal length is also

increasing the gain of the signal. The solution of such coupled equations proves that the gain is not limited by the crystal length.

3.2.5 Effective Length

(1) Aperture length

Calculate effective length of interaction by considering over what length the signal beam will walk out of the pump beam, see Figure 3-3.

$$L_a = \frac{A}{\rho} \tag{28}$$

A is the beam diameter, ρ is the walk-off angle between the two beams.

For Gaussian beams, the result is

$$L_a = \frac{\sqrt{\pi}w}{\rho} \tag{29}$$

w is the $\frac{1}{e^2}$ power radius of the Gaussian beam.

(2) Quasi-static interaction length

Due to the group velocity mismatch between pump beam and signal beam, the interaction length for parametric interaction can be quantified by the pulse splitting length, which the signal beam separates from the pump pulse in absence of gain.

$$L_{jp} = \frac{\tau}{\delta_{jp}} \ , j = s, i \tag{30}$$

where τ is the pump pulse duration, $\delta_{jp} = 1/v_{gj} - 1/v_{gp}$ is the group velocity
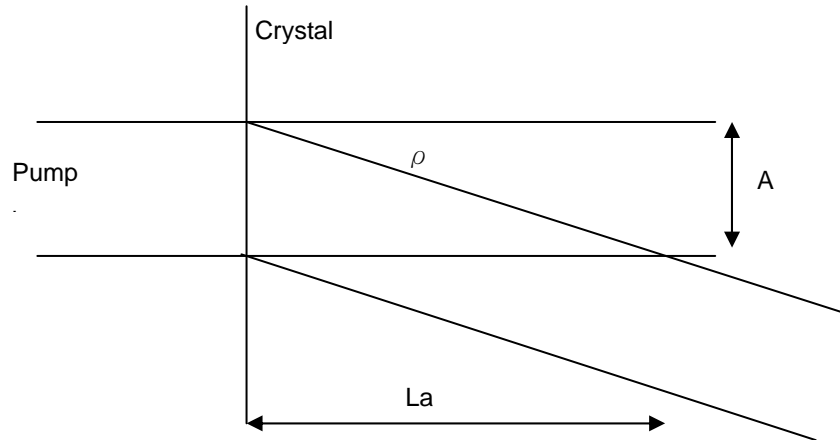
mismatch between pump and signal/idler.

Figure 3-3 : Illustration of Aperture length

3.2.6 Phase Matching and Phase Matching Bandwidth

In order to achieve maximum gain, we have to satisfy the phase matching condition,

$$\Delta \vec{k} = \vec{k}_p - \vec{k}_s - \vec{k}_i = 0 \tag{31}$$

Eq. (16) can be rewritten in the form

$$n_p = \frac{n_i \omega_i + n_s \omega_s}{\omega_p} \tag{32}$$

It is easy to show that this condition can not be satisfied in the normal dispersion region ($n_i < n_s < n_p$) of bulk isotropic materials.

For uniaxial crystal with birefringence, phase matching can be achieved by angle tuning, adjusting crystal temperature, or electro-optic effect.

Here, we take a negative crystal uniaxial crystal ($n_e < n_o$) as an example, when type-I

phase matching is achieved

$$n_{ep}(\theta_m)\omega_p = n_{os}\omega_s + n_{oi}\omega_i \tag{33}$$

In uniaxial crystals, the relation between extraordinary and ordinary refractive indexes on the propagation direction is

$$\frac{1}{n_{ep}^2(\theta_m)} = \frac{\sin^2(\theta_m)}{n_{ep}^2} + \frac{\cos^2(\theta_m)}{n_{op}^2} \tag{34}$$

n_{ep} and n_{op} are the principle refractive indexes of extraordinary and ordinary ray at wavelength λ_p.

With Eq. (33) and Eq. (34), we can derive the phase matching angle

$$\theta_m = \sin^{-1}[\frac{n_{ep}}{n_{ep}(\theta_m)}\sqrt{\frac{n_{op}^2 - n_{ep}^2(\theta_m)}{n_{op}^2 - n_{ep}^2}}] \tag{35}$$

In the frequency domain, the group velocity mismatch limits the phase matching bandwidth. We assume perfect phase matching for signal frequency ω_s, idler frequency $\omega_i = \omega_p - \omega_s$. If the signal frequency increases to $\omega_s + \Delta\omega$, so the idler frequency becomes $\omega_i - \Delta\omega$. The wave vector mismatch can be approximated to the first order as

$$\begin{aligned}\Delta k &\cong -\frac{\partial k_s}{\partial \omega_s}\Delta\omega + \frac{\partial k_i}{\partial \omega_i}\Delta\omega \\ &= \left(\frac{1}{v_{gi}} - \frac{1}{v_{gs}}\right)\Delta\omega\end{aligned} \tag{36}$$

The full width at half maximum (FWHM) phase matching bandwidth can be calculated with large gain approximation

$$\Delta\nu \cong \frac{2\sqrt{\ln 2}}{\pi}\left(\frac{\Gamma}{L}\right)^{\frac{1}{2}}\frac{1}{|\delta_{si}|} \tag{37}$$

where $\delta_{si} = \dfrac{1}{v_{gs}} - \dfrac{1}{v_{gi}}$

If the GVM between signal and idler is large, it will dramatically decrease the phase matching bandwidth. Accurately, the phase mismatch Δk should expand to the second order

$$\Delta\nu \cong \frac{2(\ln 2)^{\frac{1}{4}}}{\pi}\left(\frac{\Gamma}{L}\right)^{\frac{1}{4}}\frac{1}{\left|\dfrac{\partial^2 k_s}{\partial \omega_s^2} + \dfrac{\partial^2 k_i}{\partial \omega_i^2}\right|} \tag{38}$$

3.2.7 Theoretical prediction of THz-OPA

As introduced in Chapter 2, due to some advantages of GaSe, such as large birefringence, high nonlinearity, low absorption coefficient, we suggested that GaSe can be a good gain medium in THz-OPA.

GaSe is a birefringence crystal with sellmeier equations expressed as follows:

$$n_o^2 = 7.443 + \frac{0.405}{\lambda^2} + \frac{0.0186}{\lambda^4} + \frac{0.0061}{\lambda^6} + \frac{3.1485\lambda^2}{\lambda^2 - 2194.7} \tag{39}$$

$$n_e^2 = 5.76 + \frac{0.3879}{\lambda^2} - \frac{0.2288}{\lambda^4} + \frac{0.1223}{\lambda^6} + \frac{1.855\lambda^2}{\lambda^2 - 1780} \tag{40}$$

In order to arising OPA process, energy conservation and momentum conservation should be satisfied. Here the wavelength of pump beam is $800\,nm$, seeding beam is in terahertz range. With Eq.(2), Eq.(3) and Eq. (34), we can satisfy these condition by tuning the angle of crystal, then derive phase matching angle.

Because GaSe is a negative crystal, different polarization of incident beam can satisfy different phase matching conditions.

Type-ooe: $d_{eff} = d_{22} \cos\theta \sin 3\varphi$ (41)

Type-oee: $d_{eff} = d_{22} \cos^2\theta \cos 3\varphi$ (42)

From above two equation, d_{eff} is related to θ and φ, and conversion efficiency is proportional to the square of d_{eff}. In order to achieve higher efficiency, we can set $|\sin 3\varphi| = 1$ or $|\cos 3\varphi| = 1$ to optimize d_{eff}. In the terahertz region, we can choose Type-oee phase matching condition with collinear type OPA scheme. The corresponding external phase matching angle tuning curve is showed in Figure 3-4.
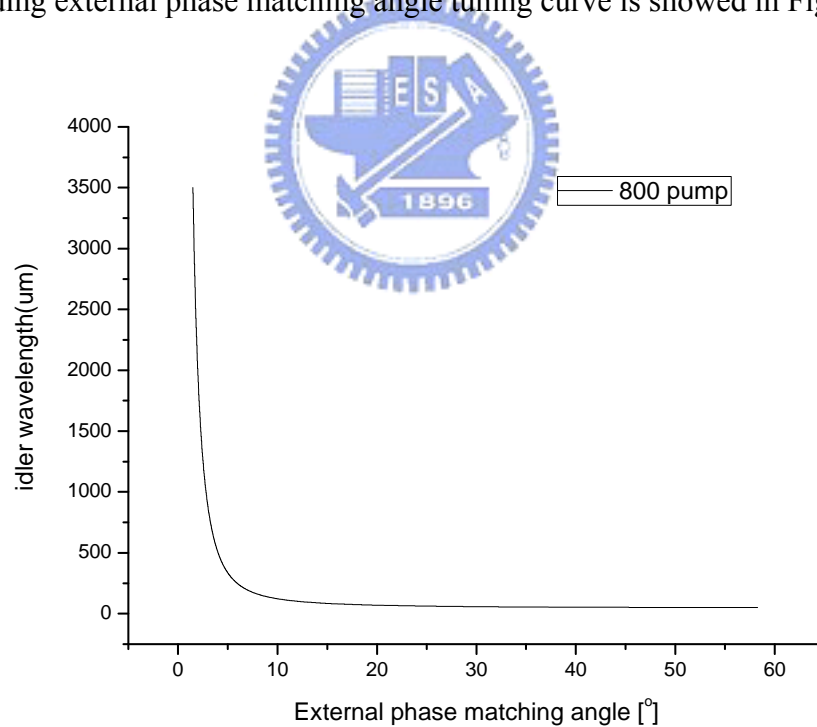

Figure 3-4 : Signal wavelength versus corresponding external phase matching angle

Group velocity mismatch (GVM) between the pump beam and the signal and (idler)

56

beam limits the interaction length over which parametric amplification takes place, while GVM between the signal and the idler beams limits the phase matching bandwidth. By calculating GVM, we can quantify interaction length by the pulse splitting length, Eq. (30). The GVM between signal, idler and pump are showed in Figure 3-5 and Figure 3-6. In our 800nm pump OPA case, the corresponding GVM are $\delta_{ip} = -9.938 \, {fs}/{mm}$, $\delta_{sp} = 464.06 \, {fs}/{mm}$ when idler wavelength at $300 \, \mu m$. They are in opposite direction with respect to the pump; in this way the signal and idler pulses tend to stay localized under the pump pulse and the gain grows exponentially even for crystal lengths well in excess of the pulse splitting length [2]. Therefore, we can increase the crystal length to raise the gain in the OPA process. For 50 fs pulse, the crystal length is about $10 \, \mu m$, for pulse duration 1 ps, the crystal length $2 \, mm$.
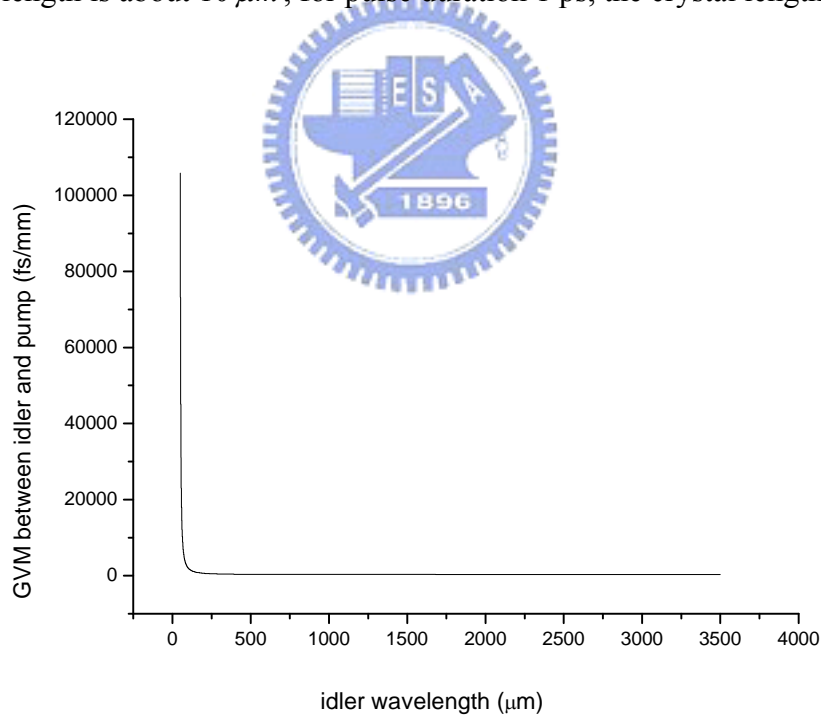

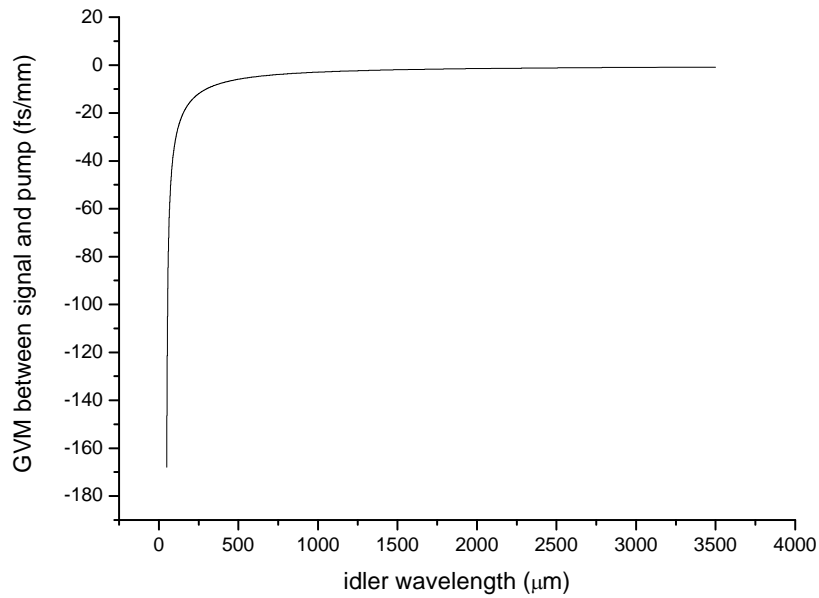Figure 3-5 : GVM between signal and pump versus signal wavelength

Figure 3-6 : GVM between idler and pump versus signal wavelength

Consider pump depletion condition and "neglecting any absorption conditions", we can calculate corresponding idler intensity, gain, and pump intensity versus to crystal length by Eq. (22), Eq. (23) and Eq. (24). The corresponding figures are shown in Figure 3-7, Figure 3-8 and Figure 3-9. From the calculating results, the gain for 800nm wavelength pumped can reach the highest gain approximately 10^6 when crystal length is sufficiently thick. However, the highest gain we can achieve in our experiment is about 4000 due to the crystal length only about $2.5\,mm$.
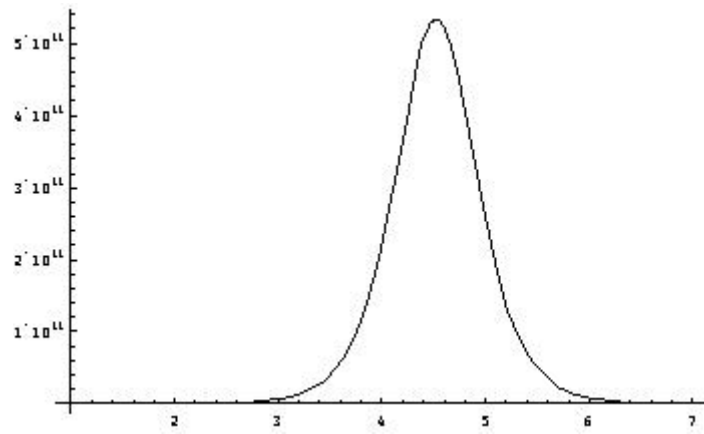
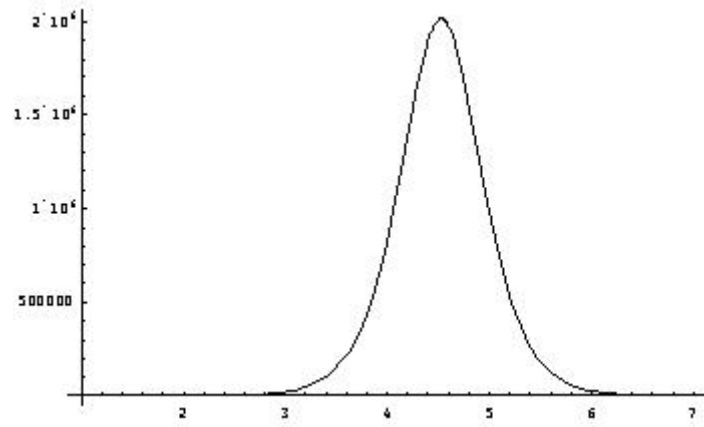Figure 3-7 : Idler intensity versus to the crystal length

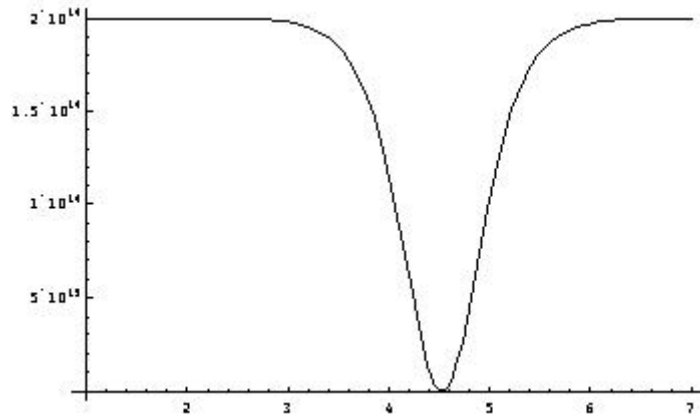Figure 3-8 : Calculated gain versus to the crystal length

Figure 3-9 : Pump intensity versus to the crystal length

3.3 Experimental Setup

3.3.1 Setup of THz-OPA

The experimental setup consists of two parts, see Figure 3-10, one is the THz-TDS the other one is the OPA stage. We use regenerated amplified laser as our light source, $1.6\,mW$, 1kHz repetition rate, pulse duration 50 fs. The first beam splitter reflects 30% of input power as THz-TDS source, transmitted 70% as OPA pump beam. The second beam splitter 90% transmitted, terahertz is generated by four wave mixing method, ionize the ambient air with laser pulses composed of both fundamental and second-harmonic waves. The residual laser beam were blocked by Teflon and terahertz beam were passed through wire-grid polarizer to make sure the polarization, finally detected by EO-sampling with $1\,mm$ thick <110> ZnTe. The electrical signal of balanced detector is connected to a lock-in amplifier in order to increase the signal/noise ratio (SNR). The terahertz radiation originally uses four-parabolic mirrors guiding to ZnTe. In order to achieve collinear OPA scheme, we use ITO as the THz dichroic mirror reflect terahertz between second and third parabolic mirror. The

OPA-pumped beam can pass through ITO, then collinearly combined with THz. In order to achieve the good temporal overlapping between the THz and the optical pumped beam, the pulse duration of the femtosecond pumped beam is stretched to about 1.5~2 ps by use of the prism pair.

Figure 3-11 is the stretched optical pumped beam. The stretched pulse duration is approximately 1.8 ps after the Gaussian fits.
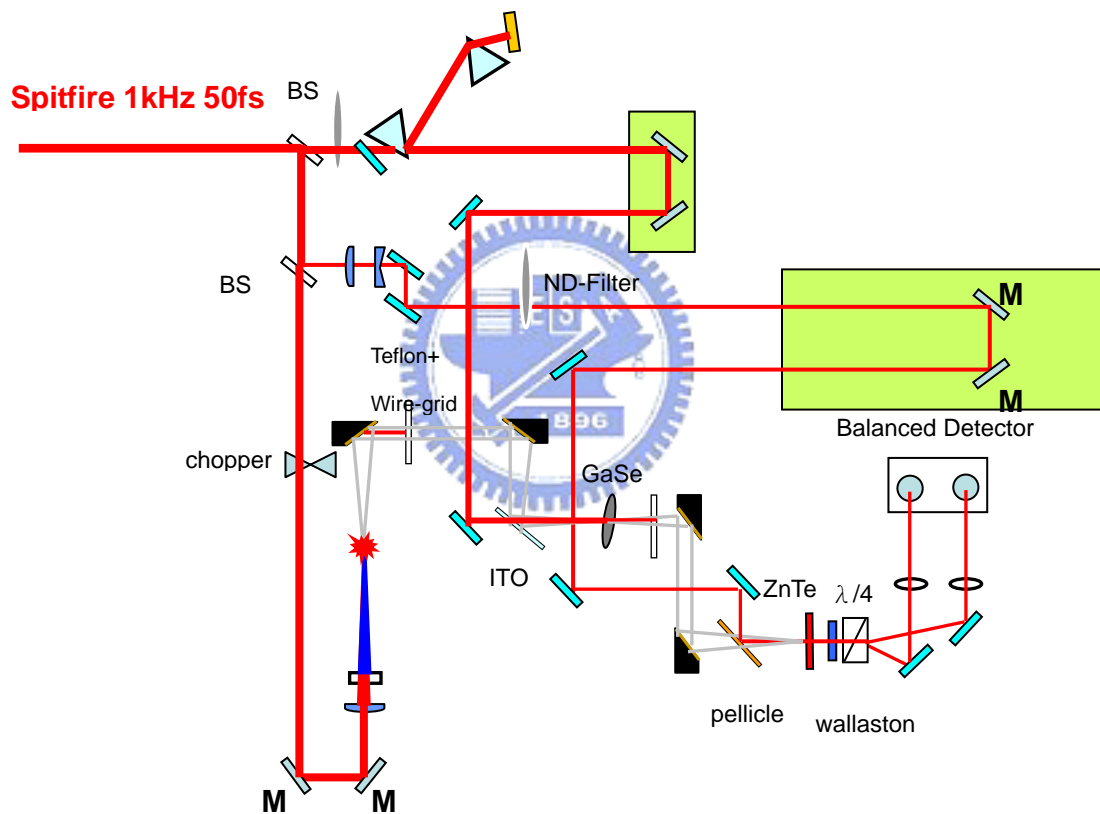

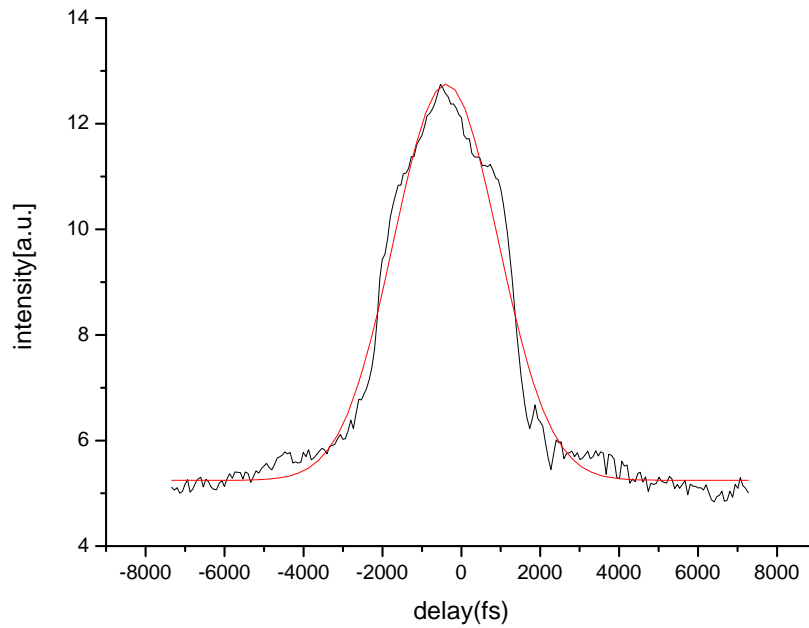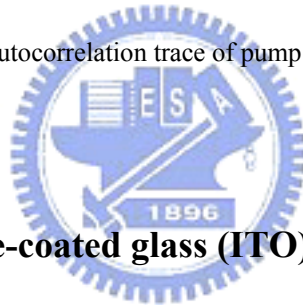Figure 3-10 : The experimental setup of THz-OPA

Figure 3-11 : The autocorrelation trace of pump beam after stretching

3.3.2 Indium–tin–oxide-coated glass (ITO)

ITO glass is widely used as a transparent conductor in thin-film display devices, such as liquid-crystal displays, solar cells, light-emitting diodes, etc. Its main feature is the combination of electrical conductivity and optical transparency. The high conductivity of ITO qualify it as a good reflector for THz radiation and its transparency at visible and near infrared wavelengths allows efficient transmission of laser radiation. ITO has high transmittance of 85% at $800\,nm$, and average reflectance about 72% at 45° in the frequency range from 0.1 to 2.5 THz. [2]

3.4 Experimental Results

During the OPA stage, we found that the measured THz signal is dramatically reduced

when the pump beam is injected. It may be due to the serious "free carrier absorption effect". Because of the energy band gap of GaSe is about $2\,eV$, the free carrier may be resulted from the two photon absorption (TPA). The TPA can strongly affect the performance of the OPA stage.

Therefore, the suitable pump intensity for OPA process is required. Figure 3-12 is the THz transmittance when the intense pumped beam is radiated on the GaSe crystal.
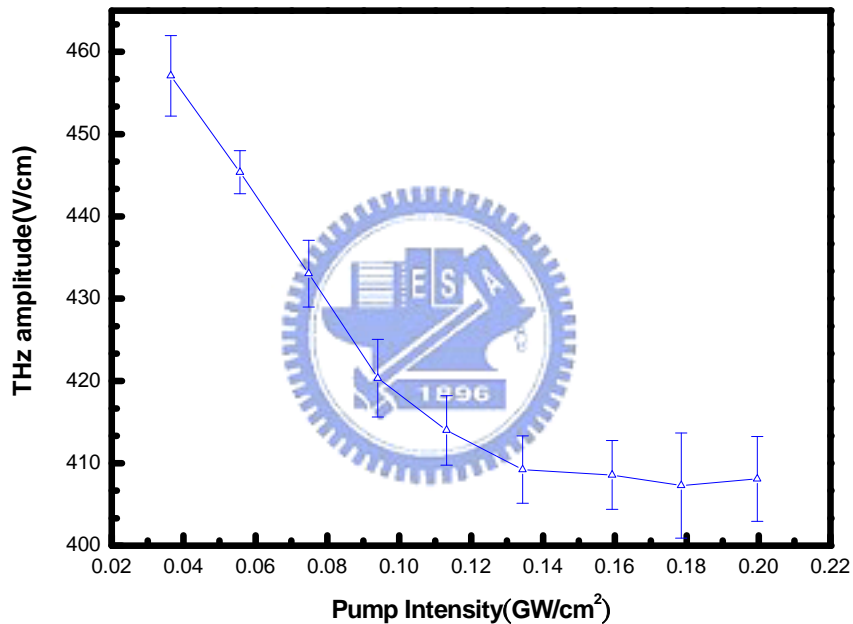

Figure 3-12 : THz transmittance versus the pump intensity

After optimizing the system, the best condition is under the pumped beam with the intensity $0.13\,GW/cm^2$. The THz amplitude is calculated to be $410\,V/cm$. The THz time domain pulse width is estimated to be about 1.5~2ps. The THz is focused by parabolic mirror on the GaSe with spot size less than $2\,mm$. Therefore, the corresponding seeding THz intensity is about 0.127 MW/cm^2.

The GaSe used in this experiment is with thickness ~3mm. According to the pump-depletion theory in OPA process, the "Gain coefficient" is described as following:

$$\sqrt{\frac{8\pi^2 (d_{eff})^2 I_p}{\lambda_s \lambda_i n_s(\theta, \lambda_s) n_i(\theta, \lambda_i) n_{op} \varepsilon_0 c}} \tag{43}$$

where I_p is the intensity of the pump beam; d_{eff} is the effective nonlinear coefficient; ε_0 is the permittivity of free space; c is the light velocity in vacuum; n_{op}, n_s, n_i are correspond to the refractive index at the pump, the generated IR wavelengths and the seeding THz wavelength; λ_s and λ_i are correspond to the wavelengths of the IR pulses and the seeding THz wavelength, respectively.

The gain coefficient versus the seeding THz wavelength is depicted as Figure 3-13. The low gain is mainly due to the low pump intensity.
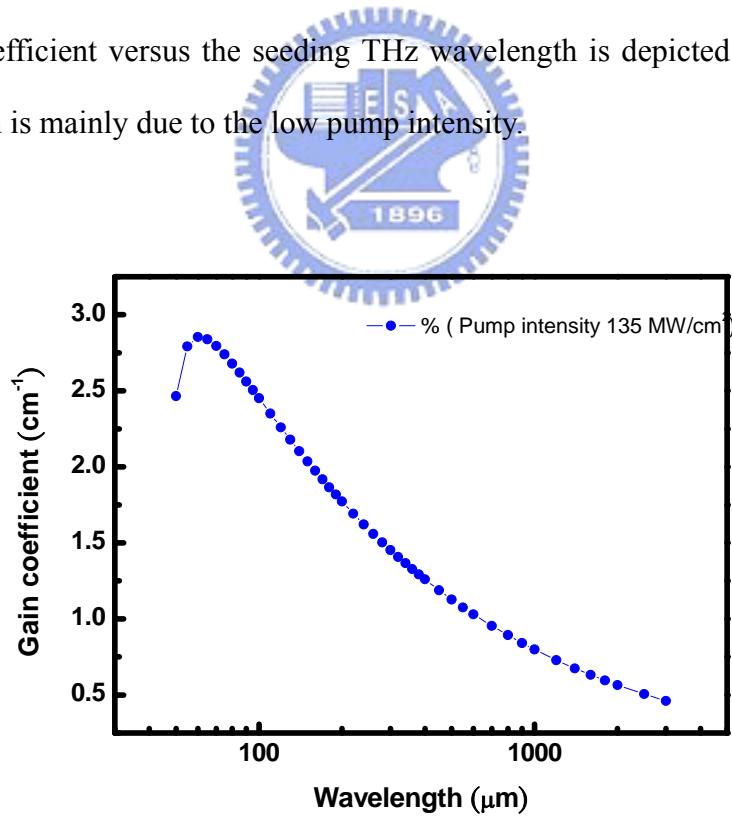

Figure 3-13 : Gain coefficient calculation

The GaSe external phase matching angles is set to be 3~5°, which corresponds to the phase matching wavelength 300~1000μm (1THz~0.3THz). The phase matching curve is shown in Figure 3-14.
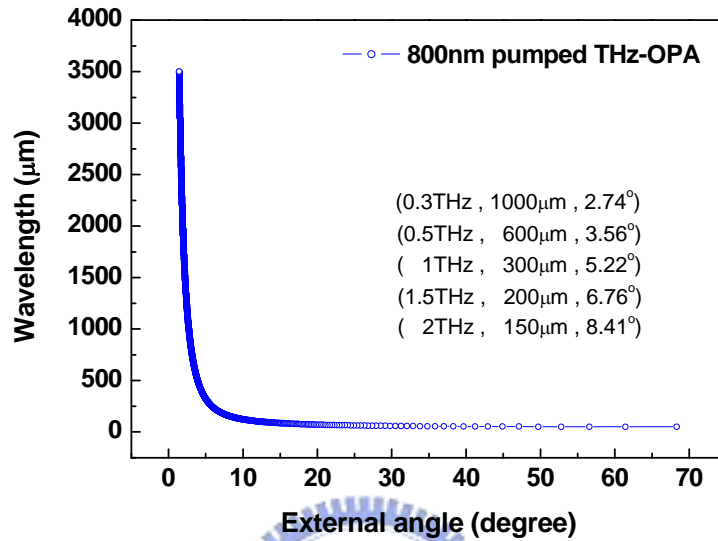

Figure 3-14 : THz-OPA phase matching curve

The seeding THz time domain profile is shown as the black-line in the Figure 3-15. The amplified THz signal is depicted as the red-line.
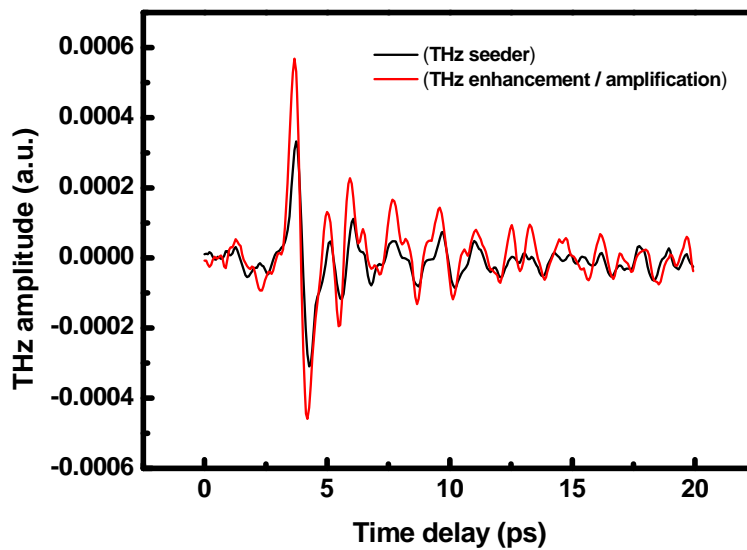
Figure 3-15 : Seeded and amplified THz time domain profile

Seeded and amplified THz spectrum is shown in Figure 3-16. The energy of weak THz signal can be enhanced 2.7 times the energy of reference THz.
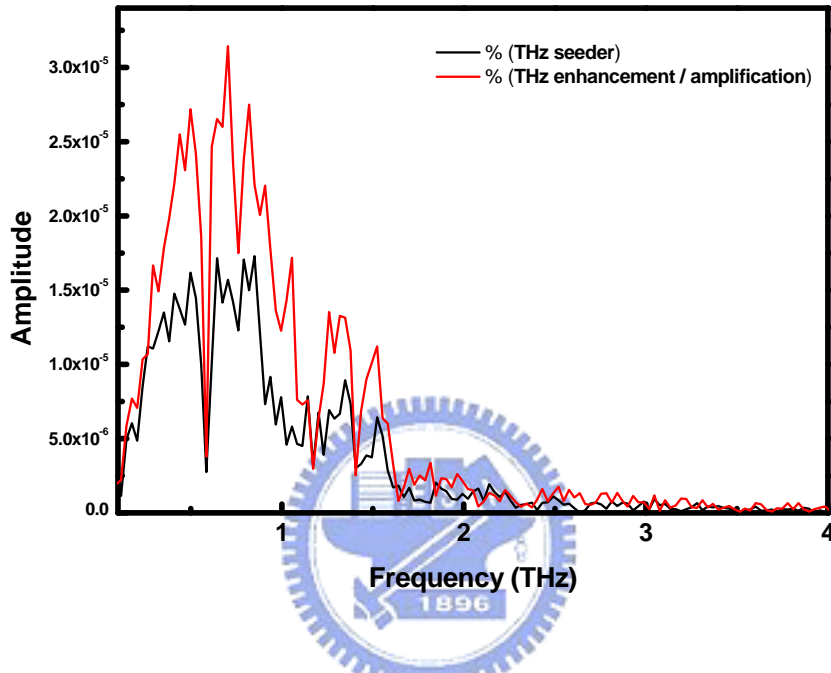

Figure 3-16 : Seeded and amplified THz spectrum

Reference

[1] http://www.physics.gatech.edu/gcuo/UltrafastOptics/UFO08Second-ordereffects.ppt

[2] G. Cerullo and S. D. Silvestri, "Ultrafast optical parametric amplifiers", Rev. Sci. Instrum. 74, 1 (2003)

[3] Indium–tin–oxide-coated glass as dichroic mirror for far-infrared electromagnetic radiation

[4]RICHARD A. BAUMGARTNER and ROBERT k. BYER, "Optical parametric amplification", IEEE JOURNAL OF QUANTUM ELECTRONICS, VOL. QE-15, NO. 6, JUNE 1979

[5]Nonlinear Optics, R.W. Boyd

Chapter 4

Conclusions and Future work

4.1   Conclusions

We successfully construct a THz-TDS system based on laser induced plasma in ambient air, and characterizing the emission. Change the angle between the fundamental beam and the second harmonic beam by varying the azimuth angle of BBO. Change the phase between fundamental beam and the second harmonic beam by varying the distance from BBO to focus point. The power dependent curve is also measured in this studies.

Optical constants of pure GaSe and 0.2% Er:GaSe, such as refractive index, absorption coefficient and conductivity are measured by THz-TDS. By use of the Lorentz-Drude model, we can extract the information of real and imaginary parts of conductivity from dielectric function, such as plasma frequency, the average momentum relaxation time and the optical phonon frequency. The mobility can be further obtained by the known extracted average momentum relaxation time.

Theoretical prediction of the THz-OPA is performed. By using the pure GaSe as the gain medium, terahertz enhancement/amplification is preliminarily performed in our studies. The gain could be as high as 150% under the phase matching condition around 1THz. Due to TPA effect, we can not use higher pumped energy or the THz will be absorbed by the generated free carriers in the crystal. From the pumped power dependent to transmitted terahertz signal, consider the absorption in the theoretical

prediction, it indeed only has small gain.

4.2 Future work

The system should be enclosed in the dry nitrogen purged. Better performance can be expected when reducing water vapor absorption of THz seeder. Due to the TPA effect of GaSe in 800 pumped OPA, we can construct a wavelength-tuning OPA system to optimize the pumped beam wavelength. The suitable wavelength should be longer than 1.3μm. Cooling the GaSe crystal to reduce the thermal effect is also another choice.

Try to find the possible gain mediums, such as PPLN, which can achieve the purpose of high power THz amplification.